Effector-triggered processing body formation attenuates host translation via ER stress responses and autophagy upon bacterial infection

Manuel González-Fuente[1,*], Nico Schulz[1], Alibek Abdrakhmanov[2,,3,], Gaiea Izzati[4], Shanshuo Zhu[1], Gautier Langin[1], Paul Gouguet[1], Mirita Franz-Wachtel[5], Boris Macek[5], Anders Hafrén[6], Yasin Dagdas[2], Suayib Üstün[1,*]

[1] Faculty of Biology and Biotechnology, Ruhr-University Bochum, Bochum, Germany

[2] Gregor Mendel Institute (GMI), Austrian Academy of Sciences, Vienna BioCenter, Vienna, Austria

[3] Vienna BioCenter PhD Program, Doctoral School of the University of Vienna and Medical University of Vienna, Vienna, Austria

[4] Center for Plant Molecular Biology (ZMBP), University of Tübingen, Tübingen, Germany

[5] Proteome Center Tübingen, Interfaculty Institute for Cell Biology, University of Tübingen, Tübingen, Germany

[6] Department of Plant Biology, Uppsala BioCenter, Swedish University of Agricultural Sciences, Uppsala, Sweden

* Correspondence: MGF (manuel.gonzalezfuente@rub.de) & SÜ (suayb.uestuen@rub.de)

Abstract

Compartmentalization of transcripts in biomolecular condensates allows rapid and cost-efficient responses to environmental stimuli. Processing bodies (P-bodies) are dynamic ribonucleoprotein condensates formed by phase separation in the cytosol. P-bodies are involved in translational arrest and mRNA decay and regulate several developmental processes and stress

responses. Pathogens have evolved strategies to exploit host degradation pathways for their own benefit, however little is known about how they impact translation. Here we show that upon infection with pathogenic bacteria *Pseudomonas syringae* pathovar *tomato* (*Pst*), P-body assembly is enhanced in an effector-dependent manner. Moreover, a P-body-defective mutant is more tolerant to bacterial infection due to altered endoplasmic reticulum (ER) stress responses, suggesting a role of P-bodies as novel susceptibility hubs. *Pst* infection is accompanied by a general host translation attenuation, which is both effector-dependent, and deregulated in the P-body-defective mutant. This indicates that P-bodies are required for the bacterial modulation of the plant translation, probably to hinder the defense responses. Additionally, host autophagy is also exploited by the bacteria to modulate P-body dynamics and its subsequent translation attenuation, revealing a complex interplay between P-body formation and disassembly during infection. Altogether, our discoveries provide novel insights on how host translation is targeted by bacteria via effector-triggered P-body formation to promote disease and uncover unknown connections between ER stress responses and autophagy with P-body dynamics.

Introduction

Maintaining a proper balance between protein synthesis and degradation is crucial for all aspects of life. Protein homeostasis, or proteostasis, determines the proper functioning of living organisms as it is key throughout all developmental stages and allows coordinated and timely responses to environmental stimuli and threats (*1*). Given this vital importance, disequilibrium of proteostasis is severely detrimental to all kinds of living organisms, from limiting cell viability in prokaryotes (*2*), to causing aging and neurodegenerative diseases in humans (*3*). It is thus not striking that proteostasis is targeted by pathogens in their efforts to modulate the host physiology to accommodate their own needs (*4*). A wide range of pathogens interfere with proteolytic pathways such as proteasomal or vacuolar degradation (*5–7*), as well as biosynthetic pathways such as transcription, translation or protein folding (*8–10*).

Plants are no exception when it comes to the importance of proteostasis. Considering the current context of climate change, an increasingly large number of environmental threats such as temperature imbalances, water unavailability, increased salinity or expanding geographic distribution of pathogens menaces the maintenance of proteostasis in plants (*11*). This does not only impact their mere ability to survive and thrive, but also inexorably affects crop yields thus threatening food security worldwide (*12*). Phytopathogens also target plant proteostasis to

promote the infection. Many pathogens modulate plant proteolytic pathways such as the ubiquitin proteasome system and associated components (*1*, *13*, *14*), endomembrane trafficking (*15*, *16*), or autophagy (*1*, *17–20*). Similarly, most stages of biosynthetic pathways are also modulated by plant pathogens, particularly viruses, as expected considering their absolute reliance on the host translation machinery (*21–24*) .Other pathogens like bacteria, oomycetes and fungi can also target protein synthesis to promote disease: from modifying chromatin accessibility (*25*) or directly hijacking the transcription machinery (*26*, *27*), to modulating the maturation and post-transcriptional processing of mRNAs (*28–30*). However, despite the reported importance of translation for mounting adequate plant defense responses (*31*), little is known about whether and how pathogens manipulate their host translation.

Mature mRNAs in eukaryotes are exported from the nucleus to the cytosol, where they are sequentially bound to different eukaryotic initiation factors (eIFs) that ultimately mediate the association with both ribosomal subunits to form translationally active polysomes (*32*). Defects in translation caused by internal cues or external stimuli such as certain types of cellular stresses, can cause the association of polysome-bound mRNAs to translation inhibitors (*33*, *34*). Translationally inactive mRNAs bind additional cytosolic proteins that mediate their phase separation into ribonucleoprotein condensates such as processing bodies (P-bodies) or stress granules, processes highly conserved among eukaryotes (*35*). In addition to the reversible sequestration of translationally inactive mRNAs (*33*), P-bodies have the particularity of harboring the mRNA decay machinery as well (*34*, *36*). P-bodies are involved in many developmental processes (*37–44*), abiotic stress responses (*43–48*), and plant-virus interactions (*23*, *49*) in animals, fungi and plants. Moreover, plant P-bodies disassemble during the first layers of plant immunity (*29*). Nevertheless, to date it remains elusive whether P-bodies can be targeted by pathogens in their efforts to modulate the host physiology to accommodate their needs.

Here we report that *Pseudomonas syringae* pathovar *tomato* (*Pst*), the causal agent of bacterial speck of tomato (*50*), deploys two effectors with liquid-like properties to induce the formation of plant P-bodies and promote disease, revealing P-bodies as a novel susceptibility hub for pathogenic bacteria. Using a P-body formation-defective mutant, we revealed that P-bodies are required for the ability of one of the P-body-inducing effectors to repress the plant endoplasmic reticulum (ER) responses and attenuate protein translation, both processes important for mounting adequate defense responses (*31*, *51*, *52*). Furthermore, we showed that autophagy is also implicated in the *Pst*-mediated formation of P-bodies and attenuation of translation,

91 revealing a so far unknown interplay between autophagy, ER stress responses and P-bodies.
92 Overall, this study uncovers a new role for P-bodies as modulators of the host protein
93 translation, and targets of effector-mediated manipulation by a pathogen.

94 **Results**

95 ***Pseudomonas syringae* induces P-body formation in an effector-dependent manner**

96 While pathogens have evolved strategies to target proteolytic pathways, it remains elusive
97 whether they can also exploit protein translation to cause disease. Considering the importance
98 of biomolecular condensates in modulating translation, we sought to investigate the behaviour
99 of P-bodies upon bacterial infection. We observed a mild reduction in the number of P-body
100 marker DCP1-GFP foci at an early stage of *Pseudomonas syringae* pathovar *tomato* strain
101 DC3000 (*Pst*) infection of *Arabidopsis thaliana* leaves (Fig. 1A). This evokes the reported P-
102 body disassembly during pathogen-associated molecular pattern (PAMP)-triggered immunity
103 (PTI)(*29*). However, a later stage of infection was marked by a significant increase in the
104 number of DCP1-GFP foci (Fig. 1A). Interestingly, this increase was compromised when using
105 the type III secretion system-defective strain Δ*hrcC* (Fig 1B), indicating that the translocation
106 of bacterial type III effector proteins was required for the increase in number of DCP1-GFP
107 foci. To rule out that this increase was caused by *Pst* ability to inhibit PTI responses, we used
108 the bacterial double Δ*avrPto/avrPtoB* mutant, which is unable to block the first stages of PTI
109 signalling (*53*). The increase in DCP1-GFP foci number was not compromised upon infection
110 with Δ*avrPto/avrPtoB* (Fig. S1A), indicating that inhibition of PTI is not the major cause of
111 *Pst*-mediated increase in DCP1-GFP foci number. Similar behaviours were observed with
112 additional GFP-tagged P-body components DCP5, VCS and LSM1A (Fig. 1C-E and S1B-C).
113 Moreover, both basal and *Pst*-induced DCP1-GFP and DCP5-GFP foci were sensitive to
114 cycloheximide (CHX; Fig. S1D-E), suggesting that these condensates are *bona fide* P-bodies
115 (*54*). Altogether, these results show that *Pst*, through its type III effectors, induces the formation
116 of Arabidopsis P-bodies.

117 **HopM1 and HopN1 induce the formation and associate with P-bodies**

118 To identify the effector(s) responsible for *Pst*-mediated increase in P-body number, ten single
119 *Pst* effectors were transiently expressed to test their individual impact on YFP-DCP1 foci
120 formation in *Nicotiana benthamiana* (Fig. 2A and S2A-B). Among the effectors screened, only
121 three showed a significant increase in YFP-DCP1 foci number: Hrp outer protein M1 (HopM1),

122 HopN1 and HopO1. For the first two, the P-body induction effect was further confirmed in a
123 more natural infection of *A. thaliana* using singly delivered effectors through an effectorless
124 *Pst* polymutant (*55*) (Fig. 2B). Additionally, in the case of HopM1, the opposite effect was
125 observed when using the single Δ*hopM1* mutant (Fig. S2C). Altogether, these results point
126 towards a specific role of certain effectors (i.e. HopM1, HopN1 and HopO1) as inducers of P-
127 body formation upon *Pst* infection.

128 To test whether the induction of P-body formation mediated by *Pst* effectors could occur in a
129 direct or indirect way, we tested if P-body-inducing effectors HopM1 and HopN1 could
130 associate with known P-body components. HA-tagged HopM1 co-immunoprecipitated with
131 YFP-DCP1 and not with DCP5-GFP, whereas HopN1-HA showed an opposite result (Fig. 2C).
132 Similarly, YFP-DCP1 foci co-localized with HopM1-RFP signal, whereas DCP5-GFP foci did
133 not (Fig. 2D). On the other hand, YFP-HopN1 foci seemed to partially co-localize with DCP1-
134 RFP foci while it co-localized with RFP-DCP5 in larger condensates (Fig. 2F). Both HopM1-
135 RFP and YFP-HopN1 presented liquid-like properties, as they both partially recovered their
136 fluorescent signal upon photobleaching (Fig. 2E & 2G). Altogether, these results suggest that
137 HopM1 and HopN1 associate specifically to different P-body components and are thus recruited
138 to P-body-like structures likely through phase separation.

139 As HopN1 is a reported cysteine protease (*56*), we tested whether its P-body inducing ability
140 was dependent on its enzymatic activity. Interestingly, a catalytic mutant version of HopN1,
141 HopN1^{D299A} (*56*), was not able to induce YFP-DCP1 foci when transiently expressed in *N.*
142 *benthamiana* (Fig. S2D-E), while partially retaining the ability to co-localize with P-bodies
143 (Fig. SF). Nevertheless, YFP-HopN1^{D299A} foci did not present liquid-like properties (Fig. S2G),
144 indicating that HopN1 protease activity might not be required to associate with P-body
145 components, but is indispensable for the recruitment of HopN1 to functional P-bodies and for
146 the increase of their number. This strengthens the notion that prokaryotic effectors can undergo
147 phase separation and that this is required for executing their proper mode of action (*57*).

148 **P-bodies are positive regulators of susceptibility via an altered endoplasmic reticulum**
149 **stress response**

150 As P-body formation was induced in a compatible interaction and is not compromised upon
151 inhibition of PTI (Fig. 1 and S1), we hypothesized that P-body formation might be a
152 consequence of the bacterial manipulation of the host to accommodate *Pst* needs, rather than a
153 plant defense response. To test this, we evaluated the bacterial multiplication in a P-body

154 formation-defective mutant *dcp5-1* (*58*). *dcp5-1* fostered a significantly lower bacterial
155 multiplication than wild-type plants when naturally infecting with *Pst* (Fig. 3A). A similar
156 pattern was observed when *Pst* was inoculated by mesophyll-infiltration, which bypasses the
157 first layers of pre-invasive immunity (Fig. S3A). Furthermore, the canonical PTI defence
158 response, flg22-induced reactive oxygen species (ROS) production, was not altered in *dcp5-1*
159 (Fig. S3B). Altogether, these results suggest that P-bodies might be positive regulators of plant
160 susceptibility and that the bacteria might actively induce their formation to their own benefit,
161 beyond immunity suppression.

162 To further investigate the role of P-bodies during infection, we conducted transcriptomic
163 analyses on the Arabidopsis PB-defective mutant *dcp5-1* and wild-type Col-0 upon infection
164 (Table 1). Generally, the effect of the mutations was minimal compared to the effect of the
165 bacterial infection, as the number of differentially expressed genes of *dcp5-1* in both mock and
166 infected conditions was considerably small (Fig. 3B). Interestingly, when we compared the
167 genes differentially regulated upon infection in both genotypes, we observed very similar
168 tendencies (Fig. 3C and S3C). Therefore, it seems that P-bodies are not responsible for major
169 changes during the transcriptional reprogramming occurring upon infection. However, when
170 carefully examining the differences between *dcp5-1* and Col-0 upon infection, we observed
171 certain pathways were distinctly regulated. For instance, abscisic acid (ABA) signalling, a
172 known susceptibility hub to *Pst* (*59*), was differentially up-regulated in *dcp5-1* as further
173 corroborated at the protein level with the ABA receptor PYRABACTIN RESISTANCE 1
174 (PYR1; Fig. S3C-D). Among the differentially down-regulated genes upon infection, we
175 observed that endoplasmic reticulum (ER) stress responsive genes were strongly down-
176 regulated in Col-0, but to a lesser extent in *dcp5-1* (Fig. 3D). This tendency was mirrored at the
177 protein level using the ER luminal BINDING PROTEIN 1 and 2 (BIP1/2) as ER stress response
178 markers (Fig. 3E). ER stress responses have emerged as novel and not-well understood
179 susceptibility hubs (*51*), and ER exit sites have been recently linked to P-body organization in
180 *Drosophila* (*60*). Therefore, we decided to further investigate the role of ER stress responses in
181 modulating P-body dynamics upon infection.

182 In coherence with the differential regulation of ER stress responses in *dcp5-1* (Fig 3D-E), this
183 mutant was found to be hypersensitive to ER stress-inducing drugs dithiothreitol (DTT) and
184 tunicamycin (TM) when applied in seedlings (Fig. S3E). Moreover, TM had a negative effect
185 on the number of YFP-DCP1 foci observed in seedling roots (Fig. S3F), evidencing a link
186 between ER stress and P-bodies in plants. Indeed, chemical induction of ER stress in adult

187 plants prevented *Pst* from inducing P-bodies (Fig. 3F and S3G). Additionally, while TM had a
188 deleterious effect in bacterial multiplication in Col-0, PB-defective *dcp5-1* showed the opposite,
189 mirroring ER stress irresponsive double mutants *bzip17/60* and *bzip28/60* (Fig. 3G) (*61*).
190 Altogether, these results points towards a deregulation of ER stress responses as a potential
191 cause of the reduced susceptibility to *Pst* of the P-body-defective *dcp5-1*, and evidence a tight
192 link between P-bodies and ER stress responses in plants, as recently suggested in animals (*62*).

193 To further investigate the strong down-regulation of ER stress responses upon infection
194 observed in Col-0 but absent in *dcp5-1* (Fig. 3D-E), and to evaluate the impact of *Pst* effectors
195 therein, we blotted ER stress response markers BIP1/2 upon infection with the wild-type and
196 effectorless polymutant *Pst* strains. As previously observed (Fig. 3E), *Pst* reduced the
197 accumulation of BIP1/2, but the effectorless polymutant did not (Fig. 3H). This suggests a role
198 for type III effectors in mediating the repression of ER stress responses. Analysing published
199 transcriptomic data of the single Δ*hopM1 Pst* mutant (*59*), we observed that ER stress
200 responsive genes were up-regulated (Fig. S3H), revealing a possible role for HopM1 as a
201 suppressor of the host ER stress responses. Previous work indicated that HopM1 associates with
202 trafficking components at the ER (*63*), strengthening our hypothesis that HopM1 may modulate
203 ER stress responses. Indeed, we confirmed that *Pst* but not Δ*hopM1* repressed several ER stress
204 responsive genes (Fig. S3I). Moreover, translocation of HopM1 alone was able to partially
205 revert the BIP1/2 accumulation triggered by the effectorless polymutant (Fig. 3H). We then had
206 a look at the subcellular localization of the ER stress responsive transcription factor BZIP28,
207 which is imported into the nucleus upon ER stress (*64*). Indeed, HopM1 reduced the nuclear
208 translocation of RFP-BZIP28 (Fig. 3I), evidencing its role as major repressor of ER stress
209 responses upon *Pst* infection, and suggesting a possible molecular mechanism for this
210 repression. Interestingly, the compromised induction of P-bodies by the Δ*hopM1* strain was not
211 observed when plants were treated with TM (Fig. S3J), suggesting that ER stress repression is
212 required for HopM1-mediated induction of P-bodies. On the other hand, HopN1 did not induce
213 any visible change in terms of ER stress responses when individually delivered through the
214 effectorless polymutant (Fig. 3I-J), suggesting that the mechanisms to induce P-bodies
215 employed by these two effectors might be different, reminiscent of their different association
216 pattern (Fig. 2C).

217 **P-bodies are required for *Pst*-mediated attenuation of the host translation**

218 To understand the role and protein composition of P-bodies during infection, different
219 proteomic approaches combining classical immunoprecipitation and proximity labelling
220 coupled with mass spectrometry were conducted to determine the protein composition of *Pst*-
221 induced P-bodies (Tables 2-3, Fig. 4A-B and S4C-D). Several known P-body components were
222 identified validating our different proteomic datasets (Fig. 4A-B and S4E). Interestingly, the
223 protein composition of *Pst*-induced P-bodies was quite different from the composition of basal
224 P-bodies (Table 2), suggesting that these biomolecular condensates are not mere "kidnappers"
225 of translationally inactive transcripts, but that they can also sequester proteins to modulate their
226 function/accessibility in the cytosol (*65*). Several proteins never previously reported to
227 associate with P-bodies were identified (Table 2). For their possible interconnections with
228 protein homeostasis, among the newly identified P-body associated proteins, we confirmed the
229 co-localization with P-body marker DCP1 and liquid-like properties of three: an
230 uncharacterized protein hereafter referred as DCP1/5-INTERACTING PROTEIN 1 (DIP1;
231 AT1G27752), the PROTEASOME SUBUNIT ALPHA TYPE 2-B (PAB2; AT1G79210) and the
232 putative E3 ligase IAN9-ASSOCIATED PROTEIN 1 (IAP1; AT1G18660; Fig. S4A-B) (*66*).

233 Additionally, several proteins with links to translation were identified in our proteomics
234 analyses (Table 3 and Fig. S4E). This is in accordance with the function of P-bodies as recruiters
235 of translationally inactive transcripts in the cytosol (*34*). To test whether *Pst*-mediated induction
236 of P-bodies had an impact on the host translation, we monitored translation activity using
237 SUrface SEnsing of Translation (SUnSET) assays (*67*). Indeed, we observed that at the same
238 timepoint at which *Pst* infection produced a major induction of P-bodies, there was a
239 considerable reduction of newly synthesized polypeptides (Fig. 4C). To evaluate whether this
240 phenomenon was caused by the sequestration of transcripts to P-bodies, we conducted a similar
241 experiment with the PB-defective mutant *dcp5-1*. Interestingly, *Pst*-mediated attenuation of
242 translation was compromised in *dcp5-1* (Fig. 4D and S4F), suggesting a possible role of P-
243 bodies in modulating general translation. As an additional proxy for evaluating general
244 translation, we monitored the phosphostatus of the RIBOSOMAL PROTEIN S6A (RPS6A).
245 RPS6A is a downstream target of the master energy sensor TARGET OF RAPAMYCIN (TOR)
246 involved in ribosome biogenesis and thus translation (*68*). Similarly to puromycin
247 incorporation, RPS6A phosphorylation was severely reduced upon *Pst* infection, but to a lesser
248 extent in *dcp5-1* (Fig. 4E and S4G), suggesting deregulation of the *Pst*-mediated attenuation of
249 translation in this background. To test whether this observed *Pst*-mediated attenuation of

250 translation was type III effector-dependent, we conducted a SUnSET assay with the effectorless
251 polymutant and single-effector-complemented strains. Indeed, the attenuation of translation
252 was reverted when inoculating the effectorless polymutant (Fig. 4F and S4H), indicating that
253 one or several effectors of *Pst* are responsible for its translational inhibition. This is coherent
254 with the reported role of translation during plant immune responses (*52*). P-body-inducing
255 effectors HopM1 and HopN1 reverted the translation induction triggered by the effectorless
256 polymutant, evidencing their role as inhibitors of translation (Fig 4F and S4H). Interestingly,
257 HopM1 was not able to repress translation in the PB-defective *dcp5-1*, indicating that HopM1
258 requires P-bodies to attenuate translation. On the other hand, HopN1 did repress translation
259 both in *dcp5-1* and Col-0, decoupling P-body formation from translation for this particular
260 effector and strengthening the notion that these two effectors might work in different and
261 complementary mechanisms. Since HopM1was shown to suppress proteasome activity by
262 inducing autophagy (*69*), we sought to investigate whether the effect of *Pst* on protein
263 translation was dependent on both degradation pathways. We observed that, *Pst*-mediated
264 attenuation of translation, evaluated by both puromycin incorporation and RPS6A
265 phosphorylation, was not majorly altered in the proteasomal mutant *rpt2a-2* (*70*), but it was
266 completely deregulated in the autophagy-deficient mutant *atg5-1* (*71*)(Fig. S4F-H). Altogether,
267 these results highlight P-bodies as possible mediators of the general attenuation of translation
268 that occurs as a virulence strategy of *Pst*.

269 ***Pst* utilizes autophagy to modulate P-body dynamics**

270 As autophagy is required to attenuate protein translation (Fig. S4F-H) and promote disease (*69*),
271 and based on a recent report linking autophagy with P-body dynamics (*72*), we sought to study
272 whether there is an interplay between these two processes upon bacterial infection in plants.
273 Using the autophagy-deficient mutant *atg5-1*, we observed an increase both basally and upon
274 *Pst* infection in the number of YFP-DCP1 foci (Fig. 5A), indicating a role of autophagy in
275 modulating P-body dynamics. This increase in YFP-DCP1 foci in *atg5-1* was accompanied by
276 an increase in protein accumulation of YFP-DCP1 (Fig. 5B and S5B), suggesting that DCP1
277 might be a target of autophagic degradation. Indeed, upon *Pst* infection, an established
278 autophagy-inducing condition (*69*), DCP1 protein levels were decreased (Fig. 5B and S5B).
279 This phenomenon was reverted when vacuolar degradation was chemically inhibited by
280 concanamycin A treatment (Fig. S5C). Moreover, YFP-DCP1 co-localizes with mCherry-
281 ATG8E-labelled autophagosomes in different autophagy-inducing conditions (Fig. 5C and
282 S5F), supporting the notion that DCP1 is a *bona fide* target of autophagic degradation. However,

283 additional P-body components DCP5, LSM1A or VCS were not visibly degraded upon *Pst*
284 infection, although DCP5 protein levels were basally stabilized in *atg5-1* (Fig. S5D-E). This
285 suggests that P-bodies, in the context of *Pst* infection, might not be targets of autophagic
286 degradation themselves, but specific components thereof might be. Interestingly, the YFP-
287 DCP1 foci observed in *atg5-1*, both in mock and infected conditions, were also considerably
288 larger in size (Fig. 5A) and insensitive to the translation inhibitor CHX (Fig. S5A-B). This
289 suggests that although increased in number, these P-bodies might not be completely functional
290 or might not sequester translationally inactive transcripts anymore. Additional lines of evidence
291 toward this hypothesis include that these enlarged P-bodies are not sensitive to neither *Pst*-
292 mediated induction nor TM-mediated repression (Fig. 5D and S5G). Furthermore, as described
293 before, although *atg5-1* is marked by an increased number of P-bodies, translation does not
294 seem to be attenuated but rather induced in this background (Fig. S4E). Interestingly, the P-
295 body- and autophagy-inducing effector HopM1 (*69*), seems to require autophagy for its
296 translational repression activity (Fig. S4G). Altogether, these results points towards a complex
297 interplay between P-bodies and autophagy, which is required for both *Pst*-mediated induction
298 of P-bodies and subsequent translation attenuation, and for their proper functioning and
299 turnover.

300 Since not all P-body components seem to be degraded via autophagy (Fig. S5E-D), suggesting
301 substrate specificity, we sought to investigate whether some of the newly identified P-body-
302 associated proteins (Fig. 4A-B and S4A-B, Table 2-3), could be also degraded via autophagy.
303 Among the described candidates, we identified DIP1 which contains a Coupling of Ubiquitin
304 conjugation to ER degradation (CUE) domain (Fig. 4A-B & S4A-B). As this domain is known
305 to bind ubiquitin (*73*), a common tag for autophagic degradation (*1*), we explored whether DIP1
306 could be involved in the interplay between autophagy and P-bodies. We confirmed that DIP1
307 co-localizes and co-immunoprecipitates with P-body components DCP1 (Fig. S4A and S5H).
308 Moreover, similarly to DCP1, DIP1 is also degraded by autophagy as its protein levels are
309 stabilized upon inhibition of vacuolar degradation or autophagy by concanamycin A treatment
310 and co-expression of AIM peptide (*74*), respectively (Fig. S5I-J). Additionally, DIP1 protein
311 levels were decreased upon chemical induction of autophagy with AZD8055 (Fig. S5K).
312 Altogether, these results show that DIP1, similarly to its associating protein DCP1, is also a
313 target of autophagic degradation and suggest that DIP1 might be involved in the interplay
314 between autophagy and P-body homeostasis.

315 **Discussion**

316 Environmental perturbations can disrupt proteostasis, negatively impacting stress responses and
317 causing proteotoxicity (*75*, *76*). To mitigate proteotoxicity, cells employ the ubiquitin-
318 proteasome system and the autophagy pathway (*1*). Additionally, eukaryotes utilize the
319 compartmentalization of translationally inactive mRNAs into cytosolic ribonucleoprotein
320 condensates such as P-bodies, providing an extra layer of regulation at the protein synthesis
321 level (*77*). Maintaining the balance between the synthesis and degradation of regulatory
322 proteins is essential to enable the induction and maintenance of stress responses. In turn,
323 pathogens have evolved strategies to manipulate the host proteostasis, particularly targeting the
324 proteasome and autophagy pathways (*5–7*, *13*, *18*, *78*), thus perturbing this balance. However,
325 how pathogens manipulate the other half of the proteostasis balance, notably at the translation
326 level, is poorly understood. Here we show that *Pst* drives an enhanced condensation of P-bodies
327 to attenuate protein translation via two effectors with liquid-like properties. Moreover, we
328 showed that *Pst*-mediated repression of ER stress response and induction of autophagy is
329 required for P-body assembly and translation attenuation (Fig. 6).

330 The ability to induce phase separation is emerging as a strategy employed by pathogens to form
331 biomolecular condensates (*79*). Recent studies indicate that pathogenic bacteria effectors
332 exhibit high propensity for phase separation and drive condensation (*57*, *80*), although their
333 exact mechanisms remain unclear. We provide novel insights into how effectors with such
334 properties might induce the condensation and assembly of P-bodies to attenuate protein
335 translation during host-microbe interactions. But why is it beneficial for the pathogen to
336 modulate a process as essential as translation? It has been shown that the modulation of other
337 aspects of proteostasis benefits pathogens. Pathogenic effectors have been shown to mimic
338 degradation pathway components (e.g., E3 ligases) to eliminate immune factors or directly
339 manipulate processes like proteasomal or autophagic degradation (*5*, *7*, *13*, *81*, *82*). However,
340 our findings provide the first evidence that bacteria can attenuate host protein translation by
341 inducing P-bodies to the pathogen own benefit. While we show that P-body induction leads to
342 translational arrest, we cannot exclude that their condensation may also sequester proteins to
343 render them nonfunctional or to neo-functionalize them, as suggested by studies on an insect
344 effector associating P-bodies with immune components to suppress plant immunity (*83*). Given
345 that protein translation is fine-tuned upon pathogen perception (*31*), it is unsurprising that
346 pathogens have evolved strategies to manipulate this process by targeting P-bodies. Our
347 findings also imply that other mechanisms are utilized by *Pst* to dampen host translation (e.g.

348 TOR activity inhibition). Future research will focus on other strategies to target host translation
349 and on identifying specific mRNAs affected in translation efficiency, potentially uncovering
350 whether they include immune components, susceptibility hubs or other pathways critical to
351 limit the infection.

352 The molecular mechanisms behind P-body assembly are less understood. For decades,
353 researchers have debated the factors driving P-body formation, which involves the aggregation
354 of smaller ribonucleoprotein particles, protein-RNA interactions, low-complexity protein
355 sequences, and liquid-liquid phase separation (*34*). While some P-body components are
356 required for their maintenance, it is unclear how they are formed or their implications in
357 pathologically relevant stress conditions (*48*). Our findings show that *Pst* triggers P-body
358 formation in an effector-dependent manner and highlight novel mechanistic insights into how
359 ER stress responses control P-body assembly. Considering the association between P-bodies
360 and the ER (*62*), as well as the role of ER contact and exit sites in regulating P-body
361 organization (*60*), targeting the ER and dampening ER stress responses appear to be efficient
362 strategies for inducing P-body assembly. Additionally, we provide evidence that *Pst*-mediated
363 induced autophagy regulates P-body assembly and disassembly, as analogously observed in
364 studies on Kaposi's sarcoma-associated herpesvirus (*84*). Emerging evidence highlights the
365 roles of the ubiquitin-proteasome system and autophagy in controlling the assembly and
366 disassembly of biomolecular condensates like stress granules and P-bodies (*85–87*). These
367 findings underscore the significance of protein degradation pathways as regulators of stress-
368 responsive biomolecular condensates.

369 But why does *Pst* degrade P-bodies? We speculate that the proper function of P-bodies requires
370 their recycling. This is supported by our observation that autophagy deficiency makes P-bodies
371 resistant to CHX treatment, which generally leads to a reduction of untranslated mRNAs (*88*).
372 P-bodies typically form only in the presence of untranslated mRNAs (*34*, *36*). As such our
373 findings strongly suggest that without recycling, P-bodies cannot effectively sequester mRNAs.
374 Alternatively, it is possible that selective autophagy of P-bodies is necessary to eliminate
375 translationally inactive mRNAs, preventing them from re-entering new cycles of translation.

376 Collectively, our study reveals that *Pst* manipulates protein translation by inducing P-body
377 condensation via the concerted action of at least two bacterial effector proteins. Utilizing these
378 effectors as cellular probes, we uncover a previously unknown connection between the ER
379 stress response and P-bodies, identifying the pathways and factors required for P-body

380 formation. Considering that protein translation and P-bodies are conserved across kingdoms,
381 our findings suggest that similar mechanisms may operate in other host-microbe interactions.

382 **Material and methods**

383 **Plant material and growth conditions**

384 *Arabidopsis thaliana* ecotype Col-0 wild-type and its derived T-DNA mutants: *dcp5-1*
385 (SALK_00881; (*58*)), *bzip17-2/60-1* (SALK_004048 & SALK_050204; (*61*)) , *bzip28-2/60-1*
386 (SALK_132285 & SALK_050204; (*61*)), *atg5-1* (SAIL_129_B07; (*71*)), *rpt2a-2*
387 (SALK_005596; (*70*)), and transgenic plants listed in Table S1, were grown under either short
388 day or long day conditions (light/dark cycles: 16h 22°C/8h 20°C, 130µmol.mm².s^{-1} light
389 intensity, 70% relative humidity) for *in vitro* experiments and seed propagation, or short day
390 conditions (light/dark cycles: 12h 22°C/ 12h 20°C, 90µmol.mm².s-1 light intensity, 70%
391 relative humidity) for bacterial infection assays. For *in vitro* experiments, seeds were sterilized
392 with 70% ethanol and sown on solid 1% sucrose-supplemented ½ Murashige and Skoog (MS)
393 medium. For experiments with adult plants, seeds were sown on individual 6-cm-diameter pots
394 filled with soil and, for infection assays, plants were grown for 4-5 weeks. Seeds for both
395 experiments *in vitro* and with adult plants were stratified for 2 days at 4ºC.

396 *Nicotiana benthamiana* plants were grown under long day conditions (light/dark cycles:
397 16h/8h, at 21°C and 70% humidity) in 6-cm-diameter individual pots filled with perlite-
398 supplemented soil for 4-6 weeks.

399 **Bacterial strains and growth conditions**

400 *Pseudomonas syringae* pathovar *tomato* wild type strain DC3000 (*89*), and its derived mutants:
401 Δ*hrcC* (*90*), Δ*avrPto/avrPtoB* (*53*), Δ*hopM1* (*91*), Δ*hopQ1* (*92*), Δ*36E::EV*, Δ*36E::hopM1* &
402 Δ*36E::hopN1* (*55*, *93*); were grown in King's B (KB) medium supplemented with 100 mg/L
403 rifampicin (plus 25 mg/L kanamycin and 50 mg/L spectinomycin for the Δ*36E* strains) at 28ºC.
404 *Agrobacterium tumefaciens* C58C1 derived strains listed in Table S2 were grown in Luria-
405 Bertani broth (LB) medium supplemented with the appropriate antibiotics (i.e. 150 mg/L
406 kanamycin, 300 mg/L gentamycin, 100 mg/L spectinomycin, 5 mg/L tetracycline and 50 mg/L
407 rifampicin) at 28ºC. *Escherichia coli* TOP10 and DB3.1 derived strains used for molecular
408 cloning with the plasmids listed in Table S3 were grown in LB medium supplemented with the
409 appropriate antibiotics (i.e. 150 mg/L kanamycin, 300 mg/L gentamycin, 100 mg/L
410 spectinomycin, 25 mg/L chloramphenicol and 50 mg/L carbenicillin).

411 **Molecular cloning**

412 The list of plasmids used and generated in this study are listed in Table S3. The list of primers
413 used to amplify the coding sequences from *A. thaliana* genes are listed in Table S4. For
414 Gateway® cloning, attB1 and attB2-flanked proof-reading PCR products were introduced into
415 entry plasmids using BP clonase™ II enzyme mix (Thermo Fisher Scientific). Expression
416 vectors were generated using LR clonaseTM II enzyme mix (Thermo Fisher Scientific).
417 Chemically competent *E. coli* TOP10 cells were transformed by heat shock (45 seconds at 42ºC,
418 2 min at 4ºC and 1h recovery at 37ºC prior to plating on antibiotic-supplemented plate). Positive
419 clones were verified by colony PCR and Sanger sequencing (Eurofins).

420 **Plant inoculation and bacterial growth assays**

421 Overnight *Pst* cultures were centrifuged for 7 minutes at 4,000 rpm. Pellets were washed twice
422 with 10 mM $MgCl_2$ prior to measuring the optical density at 600 nm (OD_{600}). For P-body
423 quantification and transcriptomic, proteomic and gene expression analyses, *Pst* inocula were
424 prepared at a final OD_{600} of 0.1 in 10 mM $MgCl_2$. For bacterial growth assays, the inocula were
425 prepared at a final OD_{600} of 0.0001 in 10 mM $MgCl_2$. The bacterial inocula were infiltrated with
426 a needleless syringe into the abaxial side of fully developed leaves from 4-5-week-old *A.*
427 *thaliana* plants. For bacterial growth assays upon dipping inoculation, the final OD_{600} was
428 adjusted to 0.1 in 10 mM MgCl2 and 0.025% Silwet L-77. Plants were fully dipped in the
429 bacterial solution for 1 minute. After inoculation, all plants were well-watered and put in
430 covered trays to reach nearly saturated humidity conditions. Unless stated otherwise, plants
431 were used for experiments 24 hours after inoculation for P-body quantification and
432 transcriptomic, proteomic and gene expression analyses, or 3 days post inoculation for bacterial
433 growth assays. Bacterial populations were estimated by plating serial dilutions of bacteria
434 extracted from two 6-mm-diameter leaf discs in 200 µL 10 mM $MgCl_2$ homogenized with a
435 tissue lyser (Retsch). Colony forming units were manually counted 48 hours after plating.

436 **Transient expression in *Nicotiana benthamiana* leaves**

437 Overnight *A. tumefaciens* cultures were centrifuged for 7 min at 4,000 rpm. Pellets were washed
438 twice with agroinfiltration buffer (10mM $MgCl_2$, 10mM MES pH 5.7) prior to measuring
439 OD_{600}. Inocula were prepared at a final OD_{600} of 0.1-0.5 in 200µM acetosyringone-
440 supplemented agroinfiltration buffer and incubated at room temperature and darkness for 2

441 hours before infiltration with a needleless syringe into the abaxial side of 4 to 6-week-old *N.*
442 *benthamiana* leaves. Plants were used for further experiments 24-48 hours after infiltration.

443 **Laser scanning confocal microscopy and image analysis**

444 Images were taken with a confocal laser scanning microscope (STELLARIS 8; Leica) using a
445 water-immersed objective (HC PL APO CS2 63×/1.20 W) with a resolution acquisition set to
446 512 x 512 (P-body quantification and FRAP analyses) or 1024 × 1024 (for subcellular
447 localization analyses) and a line average of 2-3. For GFP, excitation was set to 488 nm and
448 emission was recorded at 500–560 nm. For YFP, excitation was set to 514 nm and emission was
449 recorded at 530–570 nm. For RFP and mCherry, excitation was set to 587 nm and emission was
450 recorded at 600–640 nm. Chlorophyll autofluorescence was visualized in the far-red
451 wavelength. After acquisition, images were processed using Application Suite X (LASX; Leica)
452 and ImageJ. For clarity purposes, contrast on the individual channels was manually adjusted.
453 For P-body quantification (number and size), the analyze particle tool of ImageJ was used,
454 counting for particles whose intensity threshold were between 70 and 255 on images taken with
455 identical acquisition setup. Fluorescence recovery after photobleaching (FRAP) assays were
456 conducted using the FRAP-wizard from the Application Suite X (LASX; Leica). The recovery
457 overtime of independent photobleached foci was recorded and averaged before plotting. For
458 RFP-BZIP28 nuclear translocation analyses, several images were taken with an identical
459 acquisition setup. Afterwards, the signal around/inside every imaged nucleus was manually
460 assigned as either excluded from the nucleus or imported into the nucleus as depicted in Fig. 3.

461 **Immunoblotting**

462 Proteins were extracted in extraction buffer (100 mM Tris pH 7.5, 1 mM EDTA, 3% SDS) and
463 mixed with 4X Laemmli buffer (BioRad) prior to boiling at 95ºC for 10 minutes and clearing
464 by centrifugation of 1 minute at 13000 rpm. Total protein extracts were separated by SDS–
465 PAGE, visualized with the Stain-Free Imaging Technology in a ChemiDoc Imaging System
466 (BioRad), transferred to PVDF membranes (BioRad), blocked with 5% skimmed milk in TBS
467 (200 mM Tris and 1500 mM NaCl), for 1 hour at room temperature and incubated with the
468 correspondent antibody listed in Table S4 for 1-2 hours at room temperature or overnight at
469 4ºC. For the detection, the immunoreaction was developed using an ECL Prime Kit (GE
470 Healthcare) and detected with a ChemiDoc Imaging System (BioRad). When the Stain-Free
471 images of the total protein extracts were not taken, Ponceau S staining (0.1% Ponceau Red and
472 5% acetic acid) was performed on the membranes after revelation instead. The relative

473 quantification of the protein band intensities and ratios was performed using the Image Lab
474 software (BioRad).

475 **Co-immunoprecipitation**

476 Plant tissue was grinded with a mortar and liquid nitrogen and then extracted in 1ml/g of GTEN
477 buffer (10% glycerol, 25 mM Tris pH 7.5, 1 mM EDTA, 150 mM NaCl, 1 mM DTT, 1X
478 Protease inhibitor Cocktail (Merck) and 0.5% Triton X,). The solution was vortexed until
479 homogenized and incubated at 4ºC with rotation for 10min following centrifugation for 30
480 minutes at 4000 g and 4°C. Supernatant was filtered with three layers of Miracloth (Merck).
481 50µl of the filtrate was sampled as input, supplemented with 12.5µL Laemmli buffer 4X
482 (BioRad) and boiled for 10 minutes at 95°C. Next, 10µl/g of GFP-Trap® Agarose beads
483 (ChromoTek) were added to the remaining filtrate and incubated for 2 hours at 4ºC. The filtrates
484 were then centrifuged at 800 g for 1 minute, the supernatants were carefully removed, and the
485 pelleted beads were transferred to new 1.5mL microcentrifuge tubes in 1mL of GTEN buffer.
486 Five steps of washing were performed by centrifuging at 800 g for 1 minute using 1mL GTEN
487 buffer. After the last washing, 2X Laemmli buffer (BioRad) was added to equal amounts of
488 beads and the samples were boiled 10min at 95°C prior to immunoblotting as previously
489 described.

490 **Measurement of ROS production**

491 16 4-mm-diameter leaf discs were harvested for each condition and individually incubated
492 overnight in a 96-well plate (Pierce™; Thermo Scientific) containing 100 µL of distilled water.
493 For ROS production measurements, water was replaced by 100 µL of elicitor mix (50 nM flg22,
494 100 µM luminol, 20 µg/mL horseradish peroxidase) or mock (elicitor mix without flg22) and
495 relative luminescence was quantified in each well every minute during 1 h, using a plate reader
496 (Brand?). The total amount of luminescence per condition was calculated as the average of the
497 sums of all measurements taken during the recorder hour per sample.

498 **RNA extraction and quantitative real-time PCR**

499 Total RNA from plant samples was extracted following the manufacturer instructions with
500 either the RNeasy Plant Mini Kit (Qiagen) for RNA sequencing, or with the NucleoZOL reagent
501 (Macherey-Nagel) for the rest of applications. After extraction, 500 ng of total RNA per samples
502 were treated with DNase I (Thermo Scientific) prior to the cDNA synthesis using the
503 LunaScript® RT SuperMix Kit (New England Biolabs), in both cases following the

504 manufacturer instructions. Quantitative real-time PCR was performed using 2X MESA Blue
505 qPCR Master Mix (Eurogentec) using a 2-step protocol for 40 cycles and melting curve
506 analysis. The relative gene expression was then calculated following the ΔΔCt method.

507 **RNA sequencing**

508 Sequencing libraries were prepared from the extracted RNA using the NEBNext® Ultra™ II
509 RNA Library Prep Kit for Illumina® and Dual Index Primers (New England Biolabs) following
510 the manufacturer instructions. The quality of the libraries was verified with a Bioanalyzer
511 (Agilent) prior to send for Illumina® sequencing at the NovaSeq PE150 Platform of Novagene
512 (Cambridge, UK). After quality control, reads were mapped to the A. thaliana TAIR10 reference
513 genome. The mapped reads were counted with *htseq-count* for subsequent analysis. The $\log_2$ of
514 the fold change (log2FC) and false discovery rate (FDR) were determined using R package
515 DEseq2 (*94*) with default settings. A gene is considered significantly differentially expressed
516 when its FDR < 0.05.

517 **IP-MS/MS and proximity labelling**

518 IP-MS/MS analyses were conducted as previously described (*75*). Biotinylation test and
519 proximity labelling assays were also conducted as previously described (*95*). For the
520 downstream analysis, $\log_2$(fold change) and false discovery rate (FDR) for each protein group
521 were determined as described previously (*75*, *81*). In the case of the proximity labelling
522 proteome analysis, conduced in *N. benthamiana*, to each protein group a unique Agi-code was
523 assigned by blasting every *N. benthamiana* protein present in the protein group against *A.*
524 *thaliana* proteome and taking the most frequent Agi-code with the best E-value. An E-value
525 threshold of e^{-10} was used, in case of absence of *A. thaliana* the protein group was not considered
526 for downstream analysis.

527 **SUrface SEnsing of Translation (SUnSET) assays**

528 SUnSET assays were conducted similarly to previously described (*31*). Briefly, two 6-mm-
529 diameter-long leaf discs were individually incubated in 50 µM puromycin (Merck) in 24-well-
530 microplates for 1 hour with mild shaking. Afterwards, the two discs per sample were pooled,
531 dried with tissue paper and deep-freeze in liquid nitrogen. Protein extraction and
532 immunoblotting using anti-puromycin antibody (Merck) was conducted as previously
533 described. Relative lane intensities were calculated using the Image Lab software (BioRad).

534 **Omics downstream analysis: Gene ontology and protein Network**

535 For Gene Ontology (GO) enrichment, the lists of *A. thaliana* genes were uploaded into
536 ShinyGO software (*96*). Table of annotations was extracted for further analysis. For the
537 generation of protein networks, the lists of *A. thaliana* genes were provided to the STRING
538 database (*97*). For purposes of clarity, network nodes were manually arranged. Clusters were
539 automatically generated using the k-mean clustering tool, and representative GO terms were
540 manually assigned based on the enrichment test automatically conduced within the STRING
541 software.

542 **Data Availability**

543 The mass spectrometry data from this publication will be made available on the PRIDE archive
544 (*98*), with the identifiers PXDXXXXX and PXDXXXX. All relevant transcriptomic and
545 proteomic data are made available in the supplemental information.

546 **Acknowledgements**

547 This work was supported by Walter Benjamin Programme of the Deutsche
548 Forschungsgemeinschaft (DFG; GO 3479/1-1) to MGF. Work in the Üstün Lab was supported
549 by Emmy Noether Fellowship GZ: UE188/2-1 from the DFG and by the European Research
550 Council (ERC) under the European Union's Horizon 2020 research and innovation programme
551 (grant number 948996, DIVERSIPHAGY). We thank the confocal microscopy facility of
552 ZMBP that is supported by funds from DFG (INST 37/819-1 FUGG and INST 37/965-1 FUGG)
553 and the confocal microscopy facility of RUB (DFG Project number 523980288, GZ:INST
554 213/1180-1 FUGG).

555 **Author Contribution**

556 Conceptualization: M.G.F and S.Ü. Investigation: M.G.F, S.Ü., N.S., S.Z., G.L., G.I., P.G.
557 Visualization: M.G.F and S.Ü. Resources: A.A., A.H., Y.D., Funding acquisition: M.G.F and
558 S.Ü. Project administration: M.G.F and S.Ü. Supervision: M.G.F, S.Ü. and B.M. Writing –
559 original draft: M.G.F and S.Ü.

560 **References**

561 1. M. Raffeiner, S. Zhu, M. González-Fuente, S. Üstün, Interplay between autophagy and
562 proteasome during protein turnover. *Trends Plant Sci* **28**, 698–714 (2023).

563 2. L. Khodaparast, G. Wu, L. Khodaparast, B. Z. Schmidt, F. Rousseau, J. Schymkowitz,
564 Bacterial Protein Homeostasis Disruption as a Therapeutic Intervention. *Front Mol Biosci* **8**
565 (2021).

566 3. M. A. Thompson, E. A. De-Souza, A Year at the Forefront of Proteostasis and Aging. *Biol Open*
567 **12** (2023).

568 4. J. Yeom, D. Shin, Y. Qiao, Editorial: Protein homeostasis in host-pathogen interactions. *Front*
569 *Microbiol* **13** (2023).

570 5. Y. Jiao, J. Sun, Bacterial Manipulation of Autophagic Responses in Infection and
571 Inflammation. *Front Immunol* **10** (2019).

572 6. T. Maculins, E. Fiskin, S. Bhogaraju, I. Dikic, Bacteria-host relationship: ubiquitin ligases as
573 weapons of invasion. *Cell Res* **26**, 499–510 (2016).

574 7. Y. Choi, J. W. Bowman, J. U. Jung, Autophagy during viral infection — a double-edged sword.
575 *Nat Rev Microbiol* **16**, 341–354 (2018).

576 8. L. Gaucherand, M. M. Gaglia, The Role of Viral RNA Degrading Factors in Shutoff of Host
577 Gene Expression. *Annu Rev Virol* **9**, 213–238 (2022).

578 9. L. Neckers, U. Tatu, Molecular Chaperones in Pathogen Virulence: Emerging New Targets for
579 Therapy. *Cell Host Microbe* **4**, 519–527 (2008).

580 10. I. Mohr, N. Sonenberg, Host Translation at the Nexus of Infection and Immunity. *Cell Host*
581 *Microbe* **12**, 470–483 (2012).

582 11. B. Orosa, S. Üstün, L. I. A. Calderón Villalobos, P. Genschik, D. Gibbs, M. J. Holdsworth, E.
583 Isono, L. M. Lois, M. Trujillo, A. Sadanandom, Plant proteostasis – shaping the proteome: a
584 research community aiming to understand molecular mechanisms that control protein
585 abundance. *New Phytologist* **227**, 1028–1033 (2020).

586 12. F. L. Theodoulou, B. Orosa-Puente, M. Trujillo, V. Rubio, Plant proteostasis: a proven and
587 promising target for crop improvement. *Essays Biochem* **66**, 75–85 (2022).

588 13. G. Langin, M. González-Fuente, S. Üstün, The Plant Ubiquitin–Proteasome System as a Target
589 for Microbial Manipulation. *Annu Rev Phytopathol* **61**, 351–375 (2023).

590 14. S. Üstün, V. Bartetzko, F. Börnke, The Xanthomonas campestris Type III Effector XopJ Targets
591 the Host Cell Proteasome to Suppress Salicylic-Acid Mediated Plant Defence. *PLoS Pathog* **9**
592 (2013).

593 15. E. L. H. Yuen, S. Shepherd, T. O. Bozkurt, Traffic Control: Subversion of Plant Membrane
594 Trafficking by Pathogens. *Annu Rev Phytopathol* **61**, 325–350 (2023).

595 16. C. Brinkmann, J. Bortlik, M. Raffeiner, M. González-Fuente, L. F. Börnke, S. Üstün, F.
596 Börnke, XopM, An FFAT Motif-Containing Type III Effector Protein From Xanthomonas,
597 Suppresses MTI Responses at the Plant Plasma Membrane. *Mol Plant Pathol* **25** (2024).

598 17. M. Yang, Y. Liu, Autophagy in plant viral infection. *FEBS Lett* **596**, 2152–2162 (2022).

599 18. A. Y. Leary, N. Sanguankiattichai, C. Duggan, Y. Tumtas, P. Pandey, M. E. Segretin, J.
600 Salguero Linares, Z. D. Savage, R. J. Yow, T. O. Bozkurt, Modulation of plant autophagy
601 during pathogen attack. *J Exp Bot* **69**, 1325–1333 (2018).

602 19. J. X. Leong, G. Langin, S. Üstün, Selective autophagy: adding precision in plant immunity.
603 *Essays Biochem* **66**, 189–206 (2022).

604 20. S. Üstün, D. Hofius, Anti- and pro-microbial roles of autophagy in plant-bacteria interactions.
605 *Autophagy* **14**, 1465–1466 (2018).

606 21. D. Walsh, I. Mohr, Viral subversion of the host protein synthesis machinery. *Nat Rev Microbiol*
607 **9**, 860–875 (2011).

608 22. R. Lozano-Durán, Viral Recognition and Evasion in Plants. *Annu Rev Plant Biol* **75**, 655–677
609 (2024).

610 23. G. Hoffmann, A. Mahboubi, H. Bente, D. Garcia, J. Hanson, A. Hafrén, Arabidopsis RNA
611 processing body components LSM1 and DCP5 aid in the evasion of translational repression
612 during Cauliflower mosaic virus infection. *Plant Cell* **34**, 3128–3147 (2022).

613 24. B. Rozman, T. Fisher, N. Stern-Ginossar, Translation—A tug of war during viral infection. *Mol*
614 *Cell* **83**, 481–495 (2023).

615 25. K.-W. Ma, C. Flores, W. Ma, Chromatin Configuration as a Battlefield in Plant-Bacteria
616 Interactions. *Plant Physiol* **157**, 535–543 (2011).

617 26. A. L. Perez-Quintero, B. Szurek, A Decade Decoded: Spies and Hackers in the History of TAL
618 Effectors Research. *Annu Rev Phytopathol* **57**, 459–481 (2019).

619 27. S. Kim, C.-Y. Kim, S.-Y. Park, K.-T. Kim, J. Jeon, H. Chung, G. Choi, S. Kwon, J. Choi, J.
620 Jeon, J.-S. Jeon, C. H. Khang, S. Kang, Y.-H. Lee, Two nuclear effectors of the rice blast
621 fungus modulate host immunity via transcriptional reprogramming. *Nat Commun* **11**, 5845
622 (2020).

623 28. D. Wu, E. von Roepenack-Lahaye, M. Buntru, O. de Lange, N. Schandry, A. L. Pérez-
624 Quintero, Z. Weinberg, T. M. Lowe-Power, B. Szurek, A. J. Michael, C. Allen, S. Schillberg, T.
625 Lahaye, A Plant Pathogen Type III Effector Protein Subverts Translational Regulation to Boost
626 Host Polyamine Levels. *Cell Host Microbe* **26**, 638-649.e5 (2019).

627 29. X. Yu, B. Li, G. J. Jang, S. Jiang, D. Jiang, J. C. Jang, S. H. Wu, L. Shan, P. He, Orchestration
628 of Processing Body Dynamics and mRNA Decay in Arabidopsis Immunity. *Cell Rep* **28**, 2194-
629 2205.e6 (2019).

630 30. T. Hewezi, Phytopathogens Reprogram Host Alternative mRNA Splicing. *Annu Rev*
631 *Phytopathol* **62**, 173–192 (2024).

632 31. G. Xu, G. H. Greene, H. Yoo, L. Liu, J. Marqués, J. Motley, X. Dong, Global translational
633 reprogramming is a fundamental layer of immune regulation in plants. *Nature* **545**, 487–490
634 (2017).

635 32. K. S. Browning, J. Bailey-Serres, Mechanism of Cytoplasmic mRNA Translation. *Arabidopsis*
636 *Book* **13**, e0176 (2015).

637 33. V. Balagopal, R. Parker, Polysomes, P bodies and stress granules: states and fates of eukaryotic
638 mRNAs. *Curr Opin Cell Biol* **21**, 403–408 (2009).

639 34. Y. Luo, Z. Na, S. A. Slavoff, P-Bodies: Composition, Properties, and Functions. *Biochemistry*
640 **57**, 2424–2431 (2018).

641 35. T. Chantarachot, J. Bailey-Serres, Polysomes, stress granules, and processing bodies: A
642 dynamic triumvirate controlling cytoplasmic mRNA fate and function. *Plant Physiol* **176**, 254–
643 269 (2018).

644 36. L. D. Maldonado-Bonilla, Composition and function of P bodies in *Arabidopsis thaliana*. *Front*
645 *Plant Sci* **5**, 1–11 (2014).

37. J. Xu, J.-Y. Yang, Q.-W. Niu, N.-H. Chua, *Arabidopsis* DCP2, DCP1, and VARICOSE Form a Decapping Complex Required for Postembryonic Development. *Plant Cell* **18**, 3386–3398 (2006).

38. W. Wang, C. Wang, Y. Wang, J. Ma, T. Wang, Z. Tao, P. Liu, S. Li, Y. Hu, A. Gu, H. Wang, C. Qiu, P. Li, The P-body component DECAPPING5 and the floral repressor SISTER OF FCA regulate *FLOWERING LOCUS C* transcription in Arabidopsis. *Plant Cell* **35**, 3303–3324 (2023).

39. A. Cairo, A. Vargova, N. Shukla, C. Capitao, P. Mikulkova, S. Valuchova, J. Pecinkova, P. Bulankova, K. Riha, Meiotic exit in *Arabidopsis* is driven by P-body–mediated inhibition of translation. *Science (1979)* **377**, 629–634 (2022).

40. W. Wang, C. Wang, Y. Wang, J. Ma, T. Wang, Z. Tao, P. Liu, S. Li, Y. Hu, A. Gu, H. Wang, C. Qiu, P. Li, The P-body component DECAPPING5 and the floral repressor SISTER OF FCA regulate *FLOWERING LOCUS C* transcription in Arabidopsis. *Plant Cell* **35**, 3303–3324 (2023).

41. M. Cassani, G. Seydoux, P-body-like condensates in the germline. *Semin Cell Dev Biol* **157**, 24–32 (2024).

42. D. Teixeira, R. Parker, Analysis of P-body assembly in *Saccharomyces cerevisiae*. *Mol Biol Cell* **18**, 2274–87 (2007).

43. J.-H. Jung, J. Kim, Accumulation of P-bodies in Candida albicans under different stress and filamentous growth conditions. *Fungal Genetics and Biology* **48**, 1116–1123 (2011).

44. R. Loll-Krippleber, G. W. Brown, P-body proteins regulate transcriptional rewiring to promote DNA replication stress resistance. *Nat Commun* **8**, 558 (2017).

45. K. Motomura, Q. T. N. Le, T. Hamada, N. Kutsuna, S. Mano, M. Nishimura, Y. Watanabe, Diffuse Decapping Enzyme DCP2 Accumulates in DCP1 Foci Under Heat Stress in Arabidopsis thaliana. *Plant Cell Physiol* **56**, 107–115 (2015).

46. C. Perea-Resa, C. Carrasco-López, R. Catalá, V. Turečková, O. Novak, W. Zhang, L. Sieburth, J. M. Jiménez-Gómez, J. Salinas, The LSM1-7 Complex Differentially Regulates Arabidopsis Tolerance to Abiotic Stress Conditions by Promoting Selective mRNA Decapping. *Plant Cell* **28**, 505–520 (2016).

47. Z. Wang, Q. Yang, D. Zhang, Y. Lu, Y. Wang, Y. Pan, Y. Qiu, Y. Men, W. Yan, Z. Xiao, R. Sun, W. Li, H. Huang, H. Guo, A cytoplasmic osmosensing mechanism mediated by molecular crowding–sensitive DCP5. *Science (1979)* **386** (2024).

48. C. L. Riggs, N. Kedersha, P. Ivanov, P. Anderson, Mammalian stress granules and P bodies at a glance. *J Cell Sci* **133** (2020).

49. L. C. Reineke, R. E. Lloyd, Diversion of stress granules and P-bodies during viral infection. *Virology* **436**, 255–267 (2013).

50. X.-F. Xin, S. Y. He, *Pseudomonas syringae* pv. *tomato* DC3000: A Model Pathogen for Probing Disease Susceptibility and Hormone Signaling in Plants. *Annu Rev Phytopathol* **51**, 473–498 (2013).

51. Y. Liu, Y. Chen, B. Li, Y. Jing, S. Tian, T. Chen, Revisiting Endoplasmic Reticulum Homeostasis, an Expanding Frontier Between Host Plants and Pathogens. *Plant Cell Environ*, doi: 10.1111/pce.15344 (2024).

688 52. J. Wang, X. Zhang, G. H. Greene, G. Xu, X. Dong, PABP/purine-rich motif as an initiation
689 module for cap-independent translation in pattern-triggered immunity. *Cell* **185**, 3186-3200.e17
690 (2022).

691 53. P. He, L. Shan, N.-C. Lin, G. B. Martin, B. Kemmerling, T. Nürnberger, J. Sheen, Specific
692 bacterial suppressors of MAMP signaling upstream of MAPKKK in Arabidopsis innate
693 immunity. *Cell* **125**, 563–75 (2006).

694 54. U. Sheth, R. Parker, Decapping and Decay of Messenger RNA Occur in Cytoplasmic
695 Processing Bodies. *Science (1979)* **300**, 805–808 (2003).

696 55. H.-L. Wei, S. Chakravarthy, J. Mathieu, T. C. Helmann, P. Stodghill, B. Swingle, G. B. Martin,
697 A. Collmer, *Pseudomonas syringae* pv. *tomato* DC3000 Type III Secretion Effector
698 Polymutants Reveal an Interplay between HopAD1 and AvrPtoB. *Cell Host Microbe* **17**, 752–
699 762 (2015).

700 56. J. J. Rodríguez-Herva, P. González-Melendi, R. Cuartas-Lanza, M. Antúnez-Lamas, I. Río-
701 Alvarez, Z. Li, G. López-Torrejón, I. Díaz, J. C. Del Pozo, S. Chakravarthy, A. Collmer, P.
702 Rodríguez-Palenzuela, E. López-Solanilla, A bacterial cysteine protease effector protein
703 interferes with photosynthesis to suppress plant innate immune responses. *Cell Microbiol* **14**,
704 669–681 (2012).

705 57. Q. Liang, N. Peng, Y. Xie, N. Kumar, W. Gao, Y. Miao, MolPhase, an advanced prediction
706 algorithm for protein phase separation. *EMBO J* **43**, 1898–1918 (2024).

707 58. J. Xu, N.-H. Chua, Arabidopsis decapping 5 is required for mRNA decapping, P-body
708 formation, and translational repression during postembryonic development. *Plant Cell* **21**,
709 3270–9 (2009).

710 59. C. Roussin-Léveillée, G. Lajeunesse, M. St-Amand, V. P. Veerapen, G. Silva-Martins, K.
711 Nomura, S. Brassard, A. Bolaji, S. Y. He, P. Moffett, Evolutionarily conserved bacterial
712 effectors hijack abscisic acid signaling to induce an aqueous environment in the apoplast. *Cell*
713 *Host Microbe* **30**, 489-501.e4 (2022).

714 60. S. N. Milano, L. V Bayer, J. J. Ko, C. E. Casella, D. P. Bratu, The role of ER exit sites in
715 maintaining P-body organization and integrity during Drosophila melanogaster oogenesis.
716 *EMBO Rep*, doi: 10.1038/s44319-024-00344-x (2024).

717 61. J.-S. Kim, K. Yamaguchi-Shinozaki, K. Shinozaki, ER-Anchored Transcription Factors bZIP17
718 and bZIP28 Regulate Root Elongation. *Plant Physiol* **176**, 2221–2230 (2018).

719 62. J. E. Lee, P. I. Cathey, H. Wu, R. Parker, G. K. Voeltz, Endoplasmic reticulum contact sites
720 regulate the dynamics of membraneless organelles. *Science (1979)* **367** (2020).

721 63. S. Üstün, A. Sheikh, S. Gimenez-Ibanez, A. Jones, V. Ntoukakis, F. Börnke, The Proteasome
722 Acts as a Hub for Plant Immunity and Is Targeted by *Pseudomonas* Type III Effectors. *Plant*
723 *Physiol* **172**, 1941–1958 (2016).

724 64. J.-X. Liu, S. H. Howell, bZIP28 and NF-Y transcription factors are activated by ER stress and
725 assemble into a transcriptional complex to regulate stress response genes in Arabidopsis. *Plant*
726 *Cell* **22**, 782–96 (2010).

727 65. R. Nostramo, S. Xing, B. Zhang, P. K. Herman, Insights into the Role of P-Bodies and Stress
728 Granules in Protein Quality Control. *Genetics* **213**, 251–265 (2019).

66. Z. Chen, J. Huang, J. Li, F. L. H. Menke, J. D. G. Jones, H. Guo, Reversible ubiquitination of integrated domain controls paired NLR immune receptor complex homeostasis. [Preprint] (2024). https://doi.org/10.1101/2024.07.01.599856.

67. D. Van Hoewyk, Use of the non-radioactive SUnSET method to detect decreased protein synthesis in proteasome inhibited Arabidopsis roots. *Plant Methods* **12**, 20 (2016).

68. T. Dobrenel, E. Mancera-Martínez, C. Forzani, M. Azzopardi, M. Davanture, M. Moreau, M. Schepetilnikov, J. Chicher, O. Langella, M. Zivy, C. Robaglia, L. A. Ryabova, J. Hanson, C. Meyer, The Arabidopsis TOR Kinase Specifically Regulates the Expression of Nuclear Genes Coding for Plastidic Ribosomal Proteins and the Phosphorylation of the Cytosolic Ribosomal Protein S6. *Front Plant Sci* **7**, 1611 (2016).

69. S. Üstün, A. Hafrén, Q. Liu, R. S. Marshall, E. A. Minina, P. V. Bozhkov, R. D. Vierstra, D. Hofius, Bacteria exploit autophagy for proteasome degradation and enhanced virulence in plants. *Plant Cell* **30**, 668–685 (2018).

70. M. Ueda, K. Matsui, S. Ishiguro, R. Sano, T. Wada, I. Paponov, K. Palme, K. Okada, The *HALTED ROOT* gene encoding the 26S proteasome subunit RPT2a is essential for the maintenance of *Arabidopsis* meristems. *Development* **131**, 2101–2111 (2004).

71. A. R. Thompson, J. H. Doelling, A. Suttangkakul, R. D. Vierstra, Autophagic Nutrient Recycling in Arabidopsis Directed by the ATG8 and ATG12 Conjugation Pathways. *Plant Physiol* **138**, 2097–2110 (2005).

72. E. R. Barrow, E. Valionyte, C. R. Baxter, Y. Yang, S. Herath, W. A. O'Connell, J. Lopatecka, A. Strachan, W. Woznica, H. N. Stephenson, G. Fejer, V. Sharma, B. Lu, S. Luo, Discovery of SQSTM1/p62-dependent P-bodies that regulate the NLRP3 inflammasome. *Cell Rep* **43**, 113935 (2024).

73. G. Prag, S. Misra, E. A. Jones, R. Ghirlando, B. A. Davies, B. F. Horazdovsky, J. H. Hurley, Mechanism of Ubiquitin Recognition by the CUE Domain of Vps9p. *Cell* **113**, 609–620 (2003).

74. Y. F. Dagdas, K. Beihaj, A. Maqbool, A. Chaparro-Garcia, P. Pandey, B. Petre, N. Tabassum, N. Cruz-Mireles, R. K. Hughes, J. Sklenar, J. Win, F. Menke, K. Findlay, M. J. Banfield, S. Kamoun, T. O. Bozkurt, An effector of the irish potato famine pathogen antagonizes a host autophagy cargo receptor. *Elife* **5**, 1–23 (2016).

75. G. Langin, M. Raffeiner, D. Biermann, M. Franz-Wachtel, D. Spinti, F. Börnke, B. Macek, S. Üstün, ER-anchored protein sorting controls the fate of two proteasome activators for intracellular organelle communication during proteotoxic stress. [Preprint] (2023). https://doi.org/10.1101/2023.12.11.571118.

76. M. S. Hipp, S.-H. Park, F. U. Hartl, Proteostasis impairment in protein-misfolding and -aggregation diseases. *Trends Cell Biol* **24**, 506–514 (2014).

77. R. Parker, U. Sheth, P Bodies and the Control of mRNA Translation and Degradation. *Mol Cell* **25**, 635–646 (2007).

78. G. Langin, P. Gouguet, S. Üstün, Microbial Effector Proteins – A Journey through the Proteolytic Landscape. *Trends Microbiol* **28**, 523–535 (2020).

79. K. Chen, X. Cao, Biomolecular condensates: phasing in regulated host–pathogen interactions. *Trends Immunol*, doi: 10.1016/j.it.2024.11.010 (2024).

80. Z. Tang, S. Shi, R. Niu, Y. Zhou, Z. Wang, R. Fu, R. Mou, S. Chen, P. Ding, G. Xu, Alleviating protein-condensation-associated damage at the endoplasmic reticulum enhances plant disease tolerance. *Cell Host Microbe* **32**, 1552-1565.e8 (2024).

81. J. X. Leong, M. Raffeiner, D. Spinti, G. Langin, M. Franz-Wachtel, A. R. Guzman, J. Kim, P. Pandey, A. E. Minina, B. Macek, A. Hafrén, T. O. Bozkurt, M. B. Mudgett, F. Börnke, D. Hofius, S. Üstün, A bacterial effector counteracts host autophagy by promoting degradation of an autophagy component. *EMBO J* **41** (2022).

82. A. Y. Leary, Z. Savage, Y. Tumtas, T. O. Bozkurt, Contrasting and emerging roles of autophagy in plant immunity. *Curr Opin Plant Biol* **52**, 46–53 (2019).

83. Q. Liu, A. C. M. Neefjes, R. Kobylinska, S. T. Mugford, M. Marzo, J. Canham, M. Schuster, R. A. L. van der Hoorn, Y. Chen, S. A. Hogenhout, Aphid effectors suppress plant immunity via recruiting defence proteins to processing bodies. [Preprint] (2024). https://doi.org/10.1101/2024.11.20.624400.

84. C.-A. Robinson, G. K. Singh, M. Kleer, T. Katsademas, E. L. Castle, B. Q. Boudreau, J. A. Corcoran, Kaposi's sarcoma-associated herpesvirus (KSHV) utilizes the NDP52/CALCOCO2 selective autophagy receptor to disassemble processing bodies. *PLoS Pathog* **19**, e1011080 (2023).

85. Z. Xie, S. Zhao, Y. Tu, E. Liu, Y. Li, X. Wang, C. Chen, S. Zhai, J. Qi, C. Wu, H. Wu, M. Zhou, W. Wang, Proteasome resides in and dismantles plant heat stress granules constitutively. *Mol Cell* **84**, 3320-3335.e7 (2024).

86. Y. Gwon, B. A. Maxwell, R.-M. Kolaitis, P. Zhang, H. J. Kim, J. P. Taylor, Ubiquitination of G3BP1 mediates stress granule disassembly in a context-specific manner. *Science (1979)* **372** (2021).

87. J. R. Buchan, R.-M. Kolaitis, J. P. Taylor, R. Parker, Eukaryotic Stress Granules Are Cleared by Autophagy and Cdc48/VCP Function. *Cell* **153**, 1461–1474 (2013).

88. D. A. Santos, L. Shi, B. P. Tu, J. S. Weissman, Cycloheximide can distort measurements of mRNA levels and translation efficiency. *Nucleic Acids Res* **47**, 4974–4985 (2019).

89. D. A. Cuppels, Generation and Characterization of Tn *5* Insertion Mutations in *Pseudomonas syringae* pv. *tomato*. *Appl Environ Microbiol* **51**, 323–327 (1986).

90. J. Yuan, S. Y. He, The Pseudomonas syringae Hrp regulation and secretion system controls the production and secretion of multiple extracellular proteins. *J Bacteriol* **178**, 6399–6402 (1996).

91. J. L. Badel, K. Nomura, S. Bandyopadhyay, R. Shimizu, A. Collmer, S. Y. He, *Pseudomonas syringae* pv. *tomato* DC3000 HopPtoM (CEL ORF3) is important for lesion formation but not growth in tomato and is secreted and translocated by the Hrp type III secretion system in a chaperone-dependent manner. *Mol Microbiol* **49**, 1239–1251 (2003).

92. C. Wei, B. H. Kvitko, R. Shimizu, E. Crabill, J. R. Alfano, N. Lin, G. B. Martin, H. Huang, A. Collmer, A *Pseudomonas syringae* pv. *tomato* DC3000 mutant lacking the type III effector HopQ1-1 is able to cause disease in the model plant *Nicotiana benthamiana*. *The Plant Journal* **51**, 32–46 (2007).

93. B. Laflamme, M. M. Dillon, A. Martel, R. N. D. Almeida, D. Desveaux, D. S. Guttman, The pan-genome effector-triggered immunity landscape of a host-pathogen interaction. *Science (1979)* **367**, 763–768 (2020).

94. M. I. Love, W. Huber, S. Anders, Moderated estimation of fold change and dispersion for RNA-seq data with DESeq2. *Genome Biol* **15**, 550 (2014).

95. H. Tan, C. Shi, A. P. Macho, R. Lozano-Durán, The cartography of plant immunity: Proximity labeling puts a novel SGT1–NSL1 regulatory module on the map. *Mol Plant* **17**, 1645–1647 (2024).

96. S. X. Ge, D. Jung, R. Yao, ShinyGO: a graphical gene-set enrichment tool for animals and plants. *Bioinformatics* **36**, 2628–2629 (2020).

97. D. Szklarczyk, R. Kirsch, M. Koutrouli, K. Nastou, F. Mehryary, R. Hachilif, A. L. Gable, T. Fang, N. T. Doncheva, S. Pyysalo, P. Bork, L. J. Jensen, C. von Mering, The STRING database in 2023: protein–protein association networks and functional enrichment analyses for any sequenced genome of interest. *Nucleic Acids Res* **51**, D638–D646 (2023).

98. Y. Perez-Riverol, C. Bandla, D. J. Kundu, S. Kamatchinathan, J. Bai, S. Hewapathirana, N. S. John, A. Prakash, M. Walzer, S. Wang, J. A. Vizcaíno, The PRIDE database at 20 years: 2025 update. *Nucleic Acids Res* **53**, D543–D553 (2025).

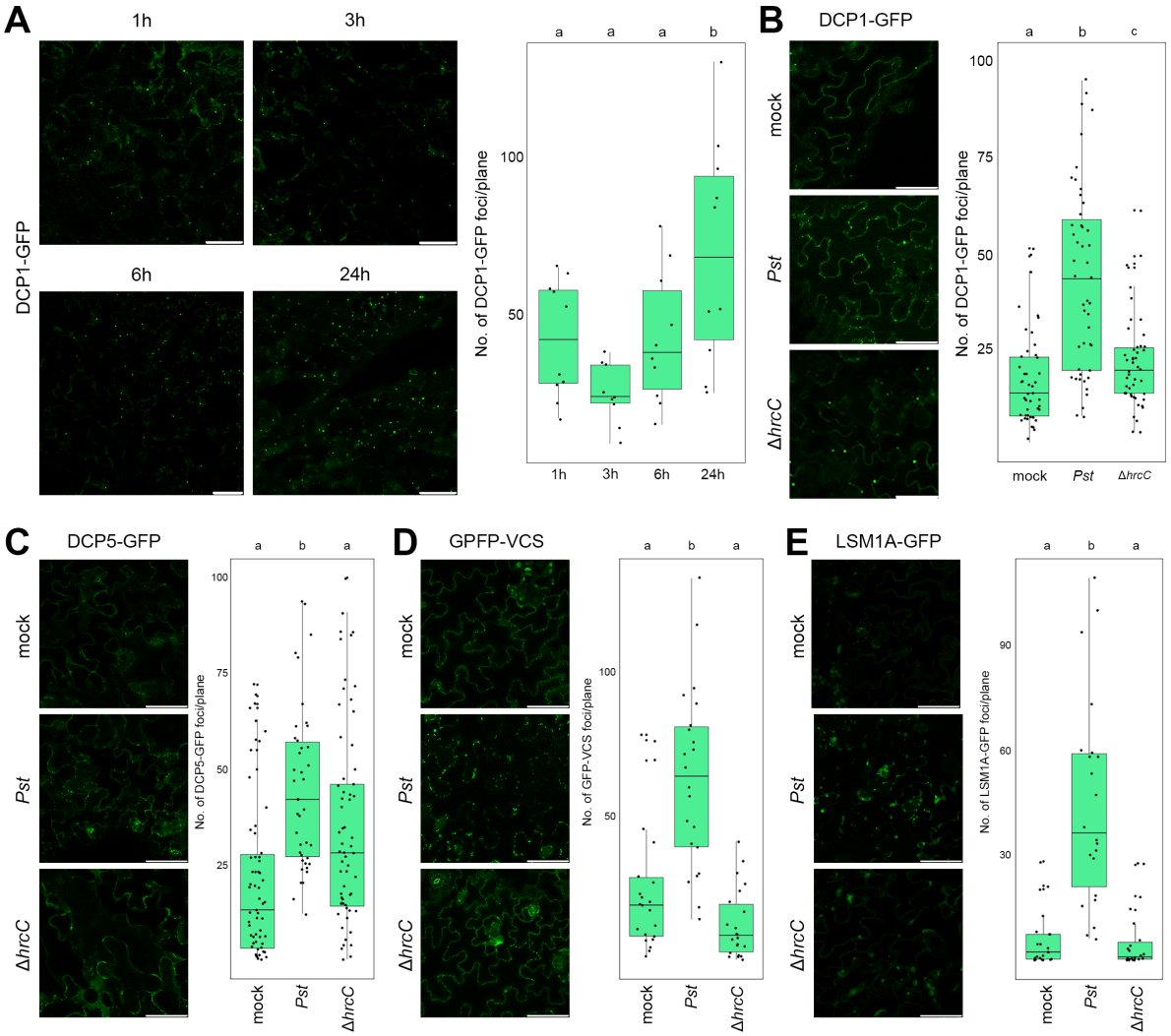

Figure 1. *Pseudomonas syringae* induces P-body formation in an effector-dependent manner.

(A-E) Confocal microscopy pictures of epidermal cells of 4-week-old *Arabidopsis thaliana* leaves expressing P-body markers DECAPPING 1 (DCP1)-GFP (A-B), DCP5-GFP (C), GFP-VARICOSE (VCS) (D) and SM-LIKE 1A (LSM1A)-GFP (E) infected with *Pseudomonas syringae* pathovar *tomato* DC3000 (*Pst*) wild-type and mutant strains or 10 mM $MgCl_2$ mock at different timepoints (A) or 24 hours (D-E) after mesophyll-infiltration at a bacterial concentration of approximately 10^7 CFUs/mL, equivalent to OD_{600}=0,1. Accompanying boxplots represent the number of fluorescent foci (particles defined by an intensity threshold of 70-255) present per focal plane from at least two independent experiments. Scale bars depict 50 µm. Different letters indicate statistical groups determined using Student *t*-test (p-value < 0.05).

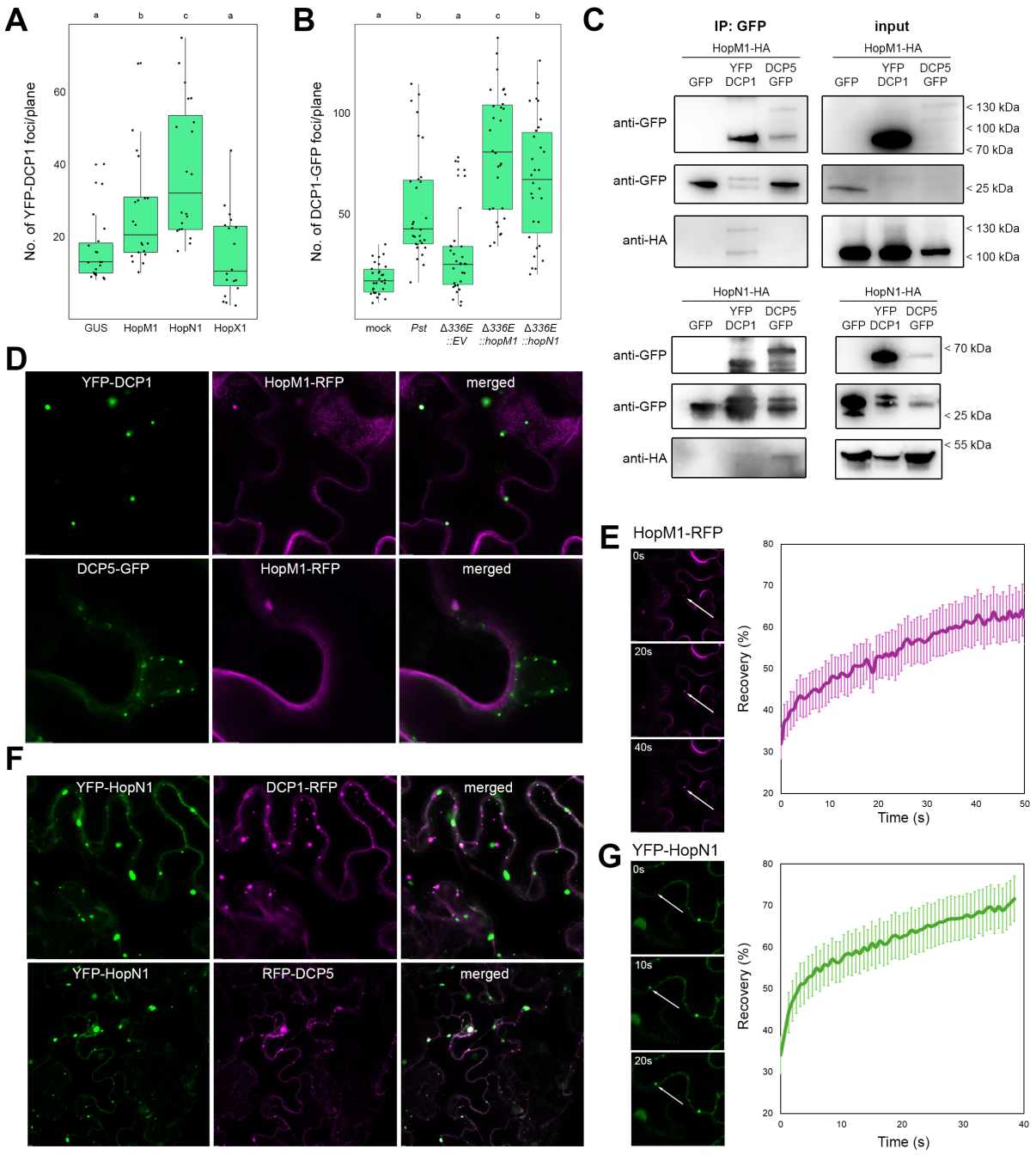

Figure 2. HopM1 and HopN1 induce the formation and associate with P-bodies.

(A-B) Boxplots representing the number of fluorescent foci per plane observed in epidermal cells of 5-week-old *N. benthamiana* leaves transiently expressing YFP-DCP1 and HA-tagged *Pst* effectors Hrp outer protein M1 (HopM1), HopN1, HopX1 or HA-tagged β-glucuronidase (GUS) as negative control (A) or 4-week-old *A. thaliana* leaves expressing DCP1-GFP infected with *Pst* wild-type and mutant strains or 10 mM $MgCl_2$ mock at 24 hours post mesophyll-infiltration with 10^7 CFUs/mL (B). Data from at least two independent experiments. Different letters indicate statistical groups determined using Student *t*-test (p-value < 0.05).

(C) Coimmunoprecipitation of YFP-DCP1, DCP5-GFP or GFP with HA-tagged HopM1 or HopN1 transiently expressed in 5-week-old *N. benthamiana* leaves 24 hours after inoculation. Total proteins (input) were subjected to immunoprecipitation (IP) with GFP-Trap beads,

854 followed by immunoblot analysis using either anti-GFP or anti-HA antibodies. GFP blot was
855 split for visualization purpose. Representative result from two independent experiments.

856 (D & F) Confocal microscopy pictures of transiently co-expressed YFP-DCP1 and DCP5-GFP
857 with HopM1-RFP (D) or DCP1-RFP and RFP-DCP5 with YFP-HopN1 (F) in 5-week-old *N.*
858 *benthamiana* epidermal cells. Images were taken 30–48 h after infiltration. Scale bars represent
859 5 μm.

860 (E & G) Representative confocal microscopy images and time-course plot of the fluorescence
861 signal recovery of HopM1-RFP (E) and YFP-HopN1 (G) foci after photobleaching. Recovery
862 was quantified as the percentage of fluorescence intensity compared to before photobleaching.
863 The data represented is the mean and error bars represent the standard error of the mean ($n >$
864 10). Scale bars represent 5 μm.

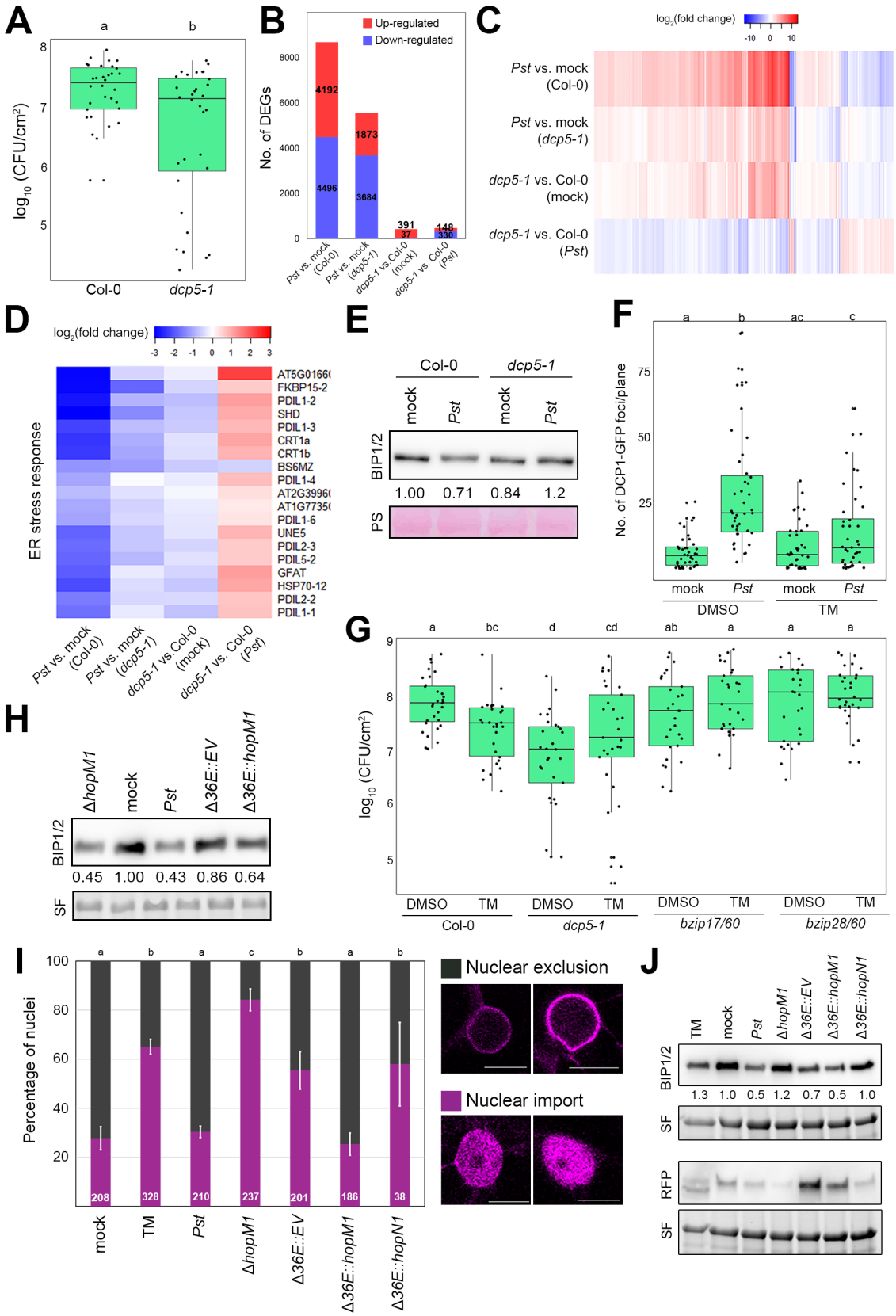

865

866 **Figure 3. P-bodies are positive regulators of susceptibility via an altered ER stress**
867 **response.**

868 (A) Bacterial population in 4-week-old *A. thaliana* leaves of wild type Col-0 and *dcp5*-1 plants
869 dipped in *Pst* solution at 10^7 CFU/mL three days post-inoculation. Data from three independent

870 experiments. Different letters indicate statistical groups determined using Student *t*-test (p-
871 value < 0.05).

872 (B) Number of differentially expressed genes (DEGs) for each condition (i.e. treatment effects:
873 *Pst* vs. mock-treated plants in Col-0 and *dcp5-1* plants, and genotype effects: *dcp5-1* vs. Col-0
874 in mock and *Pst*-treated samples). 4-week-old *dcp5-1* and Col-0 plants were mesophyll-
875 infiltrated with 10 mM $MgCl_2$ mock or 10^7 CFUs/mL *Pst* and samples were harvested 24 hours
876 after inoculation. Total number of DEGs per condition is indicated. Colors indicate the
877 proportion of DEGs up-regulated (red) and down-regulated (blue). DEGs are considered when
878 | $\log_2$(fold change) | > 1.5 and adjusted p-value < 0.05.

879 (C-D) Heatmap representing the $\log_2$(fold change) of all mapped *A. thaliana* genes (C) or a
880 fraction of ER stress response-related genes (D) for each condition in (B).

881 (E) Immunoblot analysis of ER stress response marker BINDING PROTEIN 1 and 2 (BIP1/2)
882 present in 4-week-old *A. thaliana* leaves 24 hours after mesophyll-infiltration with either 10
883 mM MgCl2 mock or 10^7 CFUs/mL *Pst*. The large subunit of the Rubisco visible after Ponceau
884 S (PS) staining serves as loading control. Numbers indicate the band intensity of the BIP1/2
885 immunoblot normalized to each sample loading.

886 (F) Boxplot representing the number of fluorescent foci per plane observed in epidermal cells
887 of 4-week-old *A. thaliana* leaves expressing DCP1-GFP infected with either 10 mM MgCl2
888 mock or 10^7 CFUs/mL *Pst* and either 10 µM tunicamycin (TM) or equivalent Dimethyl
889 sulfoxide (DMSO) volume, 24 and 8 hours prior imaging, respectively. Data from two
890 independent experiments. Different letters indicate statistical groups determined using Student
891 *t*-test (p-value < 0.05).

892 (G) Bacterial population in 4-week-old *A. thaliana* leaves of wild type Col-0 and *dcp5*-1 plants
893 mesophyll-infiltrated with *Pst* solution at 10^4 CFUs/mL and either 6 µM tunicamycin (TM) or
894 equivalent DMSO. Bacteria were extracted for counting three days post bacterial inoculation
895 and two days post TM/DMSO treatment. Data from four independent experiments. Different
896 letters indicate statistical groups determined using Student *t*-test (p-value < 0.05).

897 (H) Immunoblot analysis of ER stress response marker BIP1/2 present in 4-week-old *A.*
898 *thaliana* leaves 24 hours after mesophyll-infiltration with either 10 mM MgCl2 mock or 10^7
899 CFUs/mL of either wild-type *Pst*, single Δ*hopM1* mutant, the empty vector-complemented
900 effectorless polymutant (Δ*36E::EV*) or the *hopM1*-complemented polymutant (Δ*36E::hopM1*).
901 The large subunit of the Rubisco visible through Stain-Free imaging (BioRad) revelation serves
902 as loading control. Numbers indicate the band intensity of the BIP1/2 immunoblot normalized
903 to each sample loading.

904 (I) Stacked barplot representing the percentage of imaged nuclei based on the RFP-BZIP28
905 signal in/around them. RFP-BZIP28 was transiently expressed in 5-week-old *roq1 N.*
906 *benthamiana* leaves for 36 hours, and then mesophyll-infiltrated either 10 mM MgCl2 mock or
907 10^7 CFUs/mL of either wild-type *Pst*, single Δ*hopM1* mutant, the empty vector-complemented
908 effectorless polymutant (Δ*36E::EV*) or the *hopM1*-complemented polymutant (Δ*36E::hopM1*)
909 or 10 µM TM for 8 hours prior to imaging acquisition. Total number of nuclei per condition
910 appears at the base of the barplot. The two categories were manually assigned as "nuclear

911 excluded" (dark grey) or "nuclear imported" (magenta), as depicted in the accompanying
912 figures, based on the intensity ratio between nuclear and perinuclear regions. The scale bar
913 represents 10 µm. White error bars depict the standard error of the mean. Data from two
914 independent experiments. Different letters indicate statistical groups determined using Student
915 *t*-test (p-value < 0.05).

916 (J) Immunoblot analysis of ER stress response marker BIP1/2 and RFP-BZIP28 present in 5-
917 week-old *roq1 N. benthamiana* plants transiently expressing RFP-BZIP28 for 36 hours, and
918 then mesophyll-infiltrated either 10 mM MgCl2 mock or 10^7 CFUs/mL of either wild-type *Pst*,
919 single Δ*hopM1* mutant, the empty vector-complemented effectorless polymutant (Δ*36E::EV*)
920 or the *hopM1*-complemented polymutant (Δ*36E::hopM1*) or 10 µM TM for 8 hours prior to
921 sample harvesting. The large subunit of the Rubisco visible through Stain-Free imaging
922 (BioRad) revelation serves as loading control. Numbers below the BIP1/2 immunoblot indicate
923 the band intensity of the BIP1/2 immunoblot normalized to each sample loading.

924

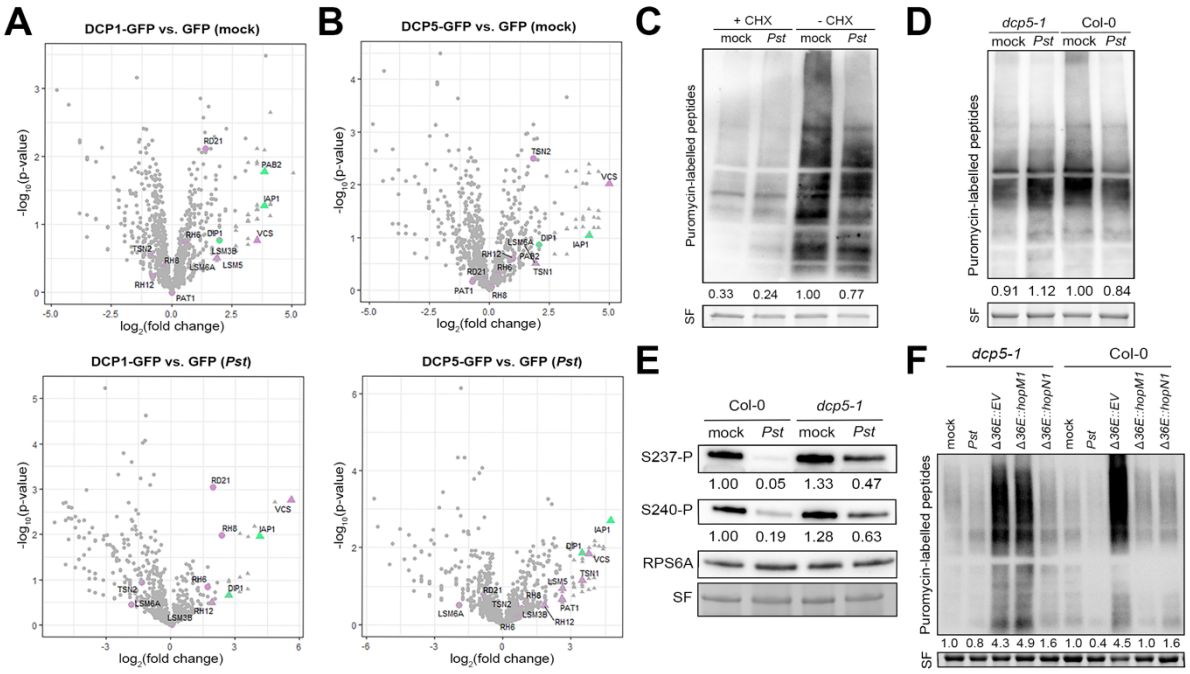

Figure 4. P-bodies are required for *Pst*-mediated attenuation of general translation.

(A-B) Volcano plots representing the results of the IP-MS/MS proteome analysis of proteins enriched in either DCP1-GFP (A) or DCP5-GFP (B)-expressing plants, compared to GFP control 24 hours upon vacuum-infiltration with either 10 mM $MgCl_2$ mock (left) or 10^7 CFUs/mL *Pst* infection. Highlighted in purple are known P-body components, and in green, candidates further studied in this work. Details are shown in Table 2.

(C) Immunoblot analysis of puromycin-labelled peptides present in 4-week-old *A. thaliana* leaves 24 hours after mesophyll-infiltration with either 10 mM MgCl2 mock or 10^7 CFUs/mL *Pst* and 4 hours after 20µM cycloheximide (CHX) or equivalent water treatment. The large subunit of the Rubisco visible through Stain-Free (SF) imaging revelation serves as loading control. Numbers indicate the lane intensity of the puromycin-labelled peptide immunoblot normalized to each sample loading.

(D) Immunoblot analysis of puromycin-labelled peptides present in 4-week-old Col-0 and *dcp5-1 A. thaliana* leaves 24 hours after mesophyll-infiltration with either 10 mM MgCl2 mock or 10^7 CFUs/mL *Pst*. The large subunit of the Rubisco visible through Stain-Free (SF) imaging revelation serves as loading control. Numbers indicate the lane intensity of the puromycin-labelled peptide immunoblot normalized to each sample loading.

(E) Immunoblot analysis of the phosphorylation status at Ser237 and Ser240 of RIBOSOMAL PROTEIN S6A (RPS6A) in 4-week-old Col-0 and *dcp5-1 A. thaliana* leaves 24 hours after mesophyll-infiltration with either 10 mM MgCl2 mock or 10^7 CFUs/mL *Pst*. The large subunit of the Rubisco visible through Stain-Free (SF) imaging revelation serves as loading control. Numbers indicate the band intensity ratios between the phosphorylation-specific RPS6A immunoblots and its respective phosphorylation-insensitive RPS6A blots, normalized to each sample loading.

950 (F) Immunoblot analysis of puromycin-labelled peptides present in 4-week-old Col-0 and *dcp5-*
951 *1 A. thaliana* leaves 24 hours after mesophyll-infiltration with either 10 mM MgCl2 mock or
952 CFUs/mL of either wild-type *Pst*, the empty vector-complemented effectorless polymutant
953 (Δ*36E::EV*) or the *hopM1*- and *hopN1*-complemented polymutant (Δ*36E::hopM1* and
954 Δ*36E::hopN1* respectively). The large subunit of the Rubisco visible through Stain-Free (SF)
955 imaging revelation serves as loading control. Numbers indicate the lane intensity of the
956 puromycin-labelled peptide immunoblot normalized to each sample loading.

957

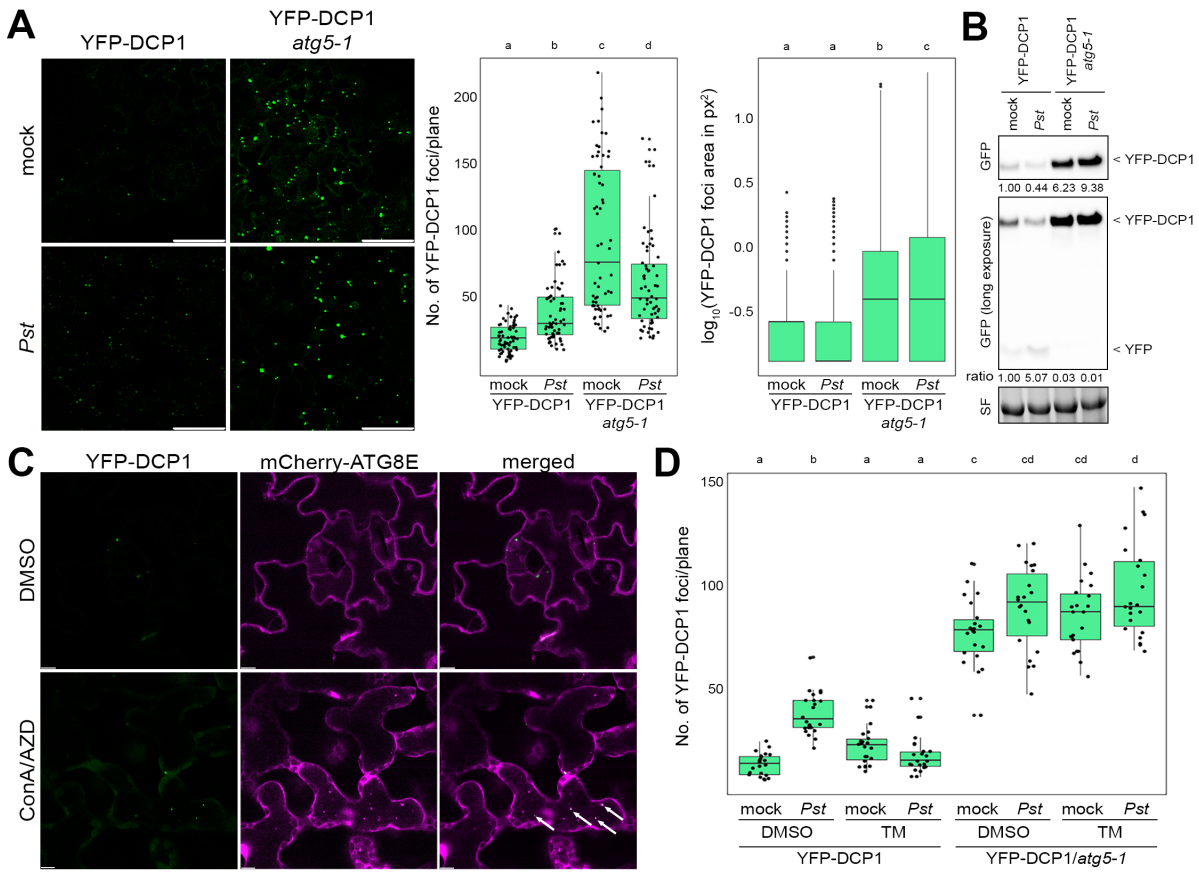

Figure 5. *Pst* utilizes autophagy to modulate P-body dynamics.

(A) Confocal microscopy pictures and boxplots representing the number and size of fluorescent foci per plane observed in epidermal cells of 4-week-old *A. thaliana* leaves expressing YFP-DCP1 in the Col-0 and *atg5-1* background at 24 hours post mesophyll-infiltration with 10^7 CFUs/mL *Pst* or 10 mM $MgCl_2$. Scale bars depict 50 µm. Data from two independent experiments. Different letters indicate statistical groups determined using Student *t*-test (p-value < 0.05).

(B) Immunoblot analysis of YFP-tagged protein levels in 4-week-old *A. thaliana* leaves expressing YFP-DCP1 in the Col-0 and *atg5-1* background mesophyll-infiltrated with 10 mM $MgCl_2$ mock or 10^7 CFUs/mL *Pst* at 24 hours post mesophyll-infiltration. The large subunit of the Rubisco visible through Stain-Free (SF) imaging revelation serves as loading control. Number indicate the band intensity of YFP-DCP1 normalized to each sample loading (top) and the ratio of YFP/YFP-DCP1 band intensity, also normalized to each sample loading (bottom).

(C) Confocal microscopy pictures of epidermal cells of 4-week-old *A. thaliana* leaves expressing YFP-DCP1 and mCherry-ATG8E mesophyll-infiltrated with 10 mM $MgCl_2$ mock or 10^7 CFUs/mL *Pst* 24 hours prior imaging. Scale bars depict 5 µM. White arrows highlight co-localization of YFP-DCP1 and mCherry-ATG8E foci.

(D) Quantification of the number of fluorescent foci per plane observed in epidermal cells of 4-week-old *A. thaliana* leaves expressing YFP-DCP1 in the Col-0 and *atg5-1* background infected with either 10 mM $MgCl_2$ mock or 10^7 CFUs/mL *Pst* 24 hours before imaging, and 6 µM TM or equivalent DMSO volume 8 hours before imaging. Data from two independent

experiments. Different letters indicate statistical groups determined using Student *t*-test (p-value < 0.05).

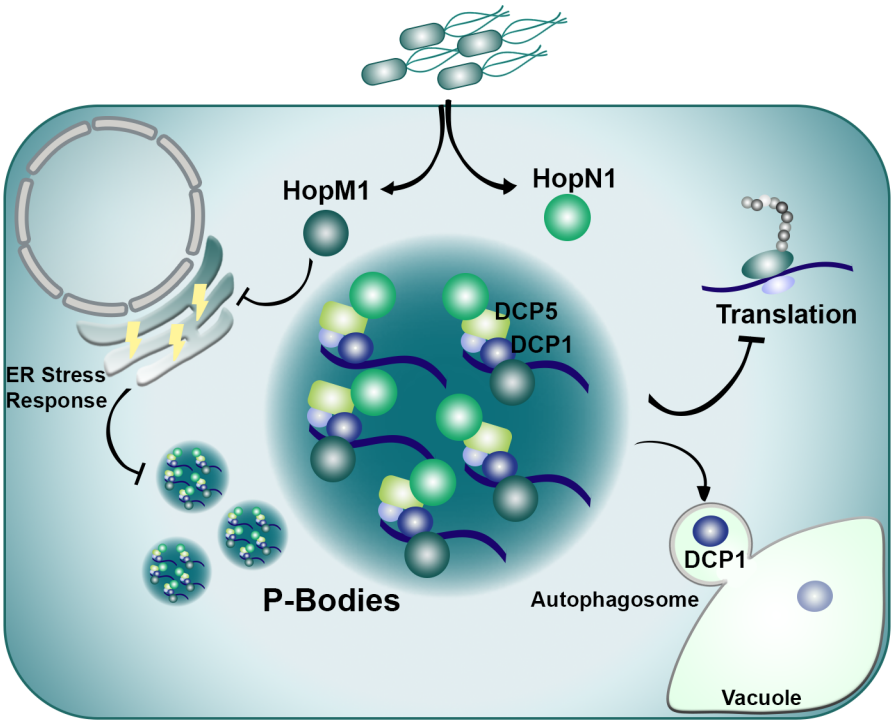

982

983 **Figure 6. Model for *Pst*-mediated induction of P-body formation and attenuation of**
984 **translation.**

985 *Pst* translocates effectors HopM1 and HopN1 that associate with host P-body components
986 DCP1 and DCP5 respectively, to induce P-body assembly and attenuate protein translation.
987 Additionally, *Pst* represses the host ER stress responses and induces autophagy, both processes
988 required for induction of P-bodies and translation attenuation.

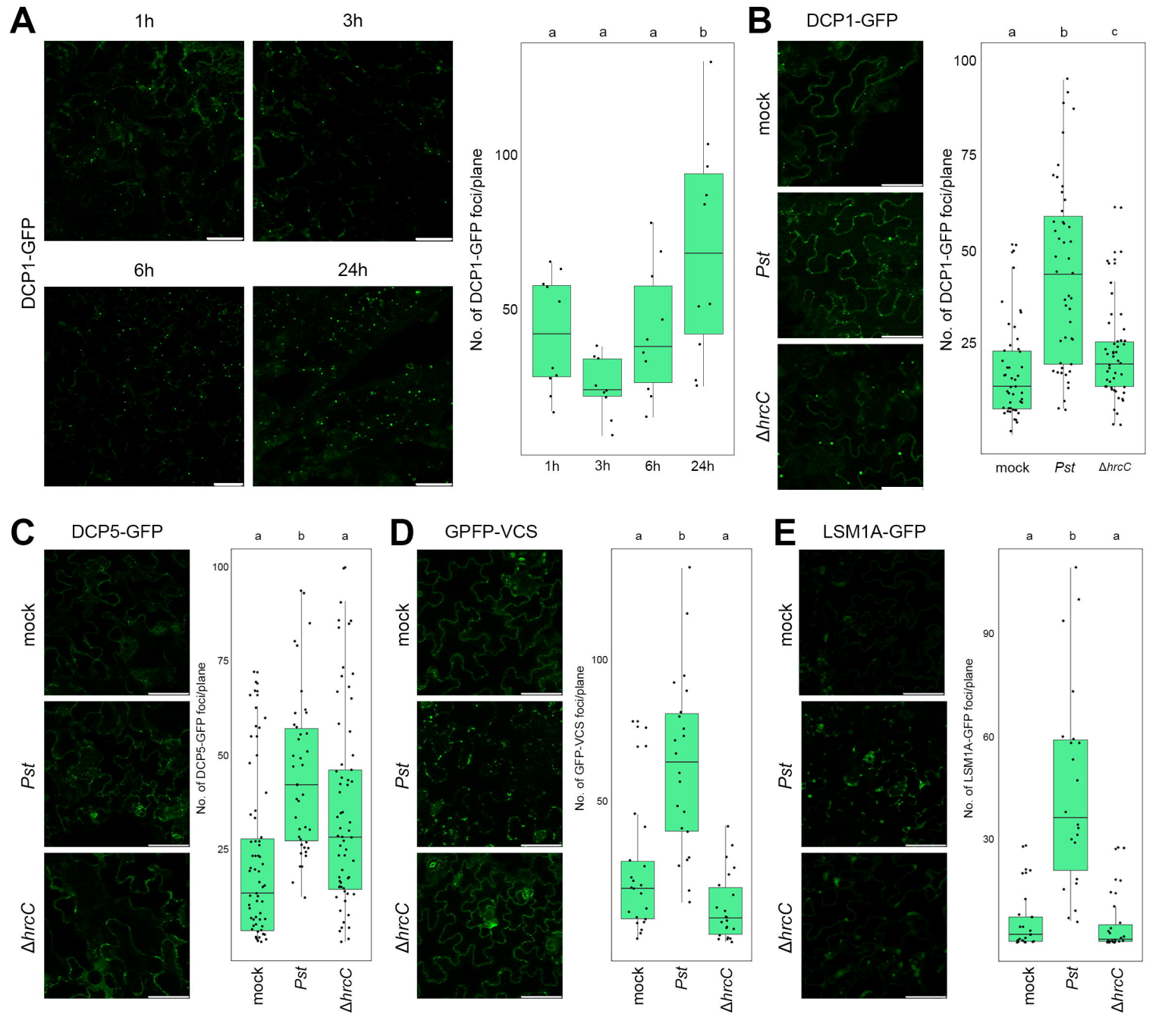
A
1h
3h
6h
24h
DCP1-GFP
No. of DCP1-GFP foci/plane
a a a b
1h 3h 6h 24h
B
DCP1-GFP
mock
Pst
ΔhrcC
a b c
No. of DCP1-GFP foci/plane
mock Pst ΔhrcC
C
DCP5-GFP
mock
Pst
ΔhrcC
a b a
No. of DCP5-GFP foci/plane
mock Pst ΔhrcC
D
GPFP-VCS
mock
Pst
ΔhrcC
a b a
No. of GFP-VCS foci/plane
mock Pst ΔhrcC
E
LSM1A-GFP
mock
Pst
ΔhrcC
a b a
No. of LSM1A-GFP foci/plane
mock Pst ΔhrcC

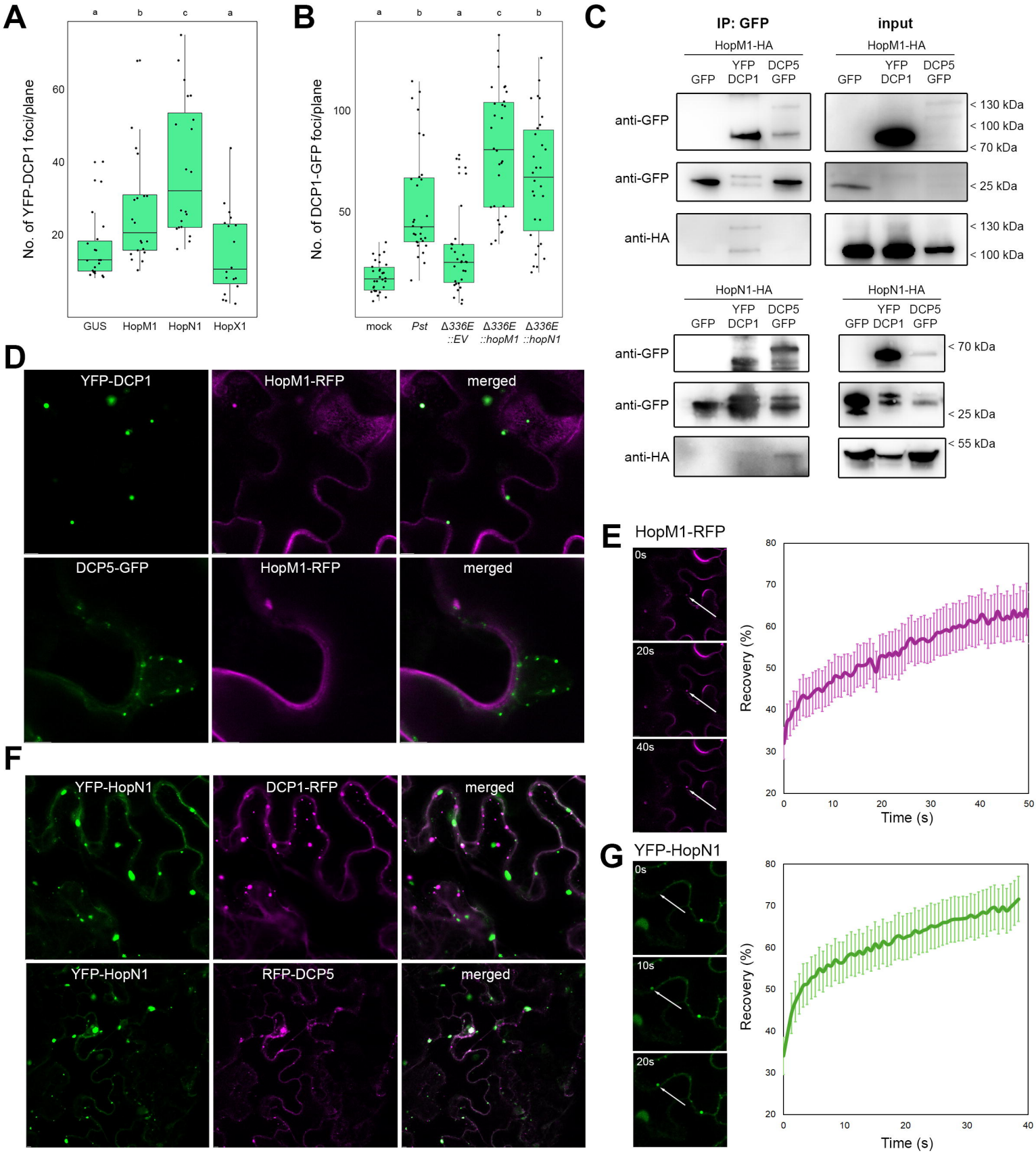
A
a b c a
No. of YFP-DCP1 foci/plane
60
40
20
GUS
HopM1
HopN1
HopX1
B
a b a c b
No. of DCP1-GFP foci/plane
100
50
mock
Pst
Δ336E ::EV
Δ336E ::hopM1
Δ336E ::hopN1
C
IP: GFP
input
HopM1-HA
GFP
YFP DCP1
DCP5 GFP
anti-GFP
anti-HA
< 130 kDa
< 100 kDa
< 70 kDa
< 25 kDa
HopN1-HA
< 55 kDa
D
YFP-DCP1
HopM1-RFP
merged
DCP5-GFP
E
HopM1-RFP
0s
20s
40s
Recovery (%)
Time (s)
F
YFP-HopN1
DCP1-RFP
RFP-DCP5
G
10s

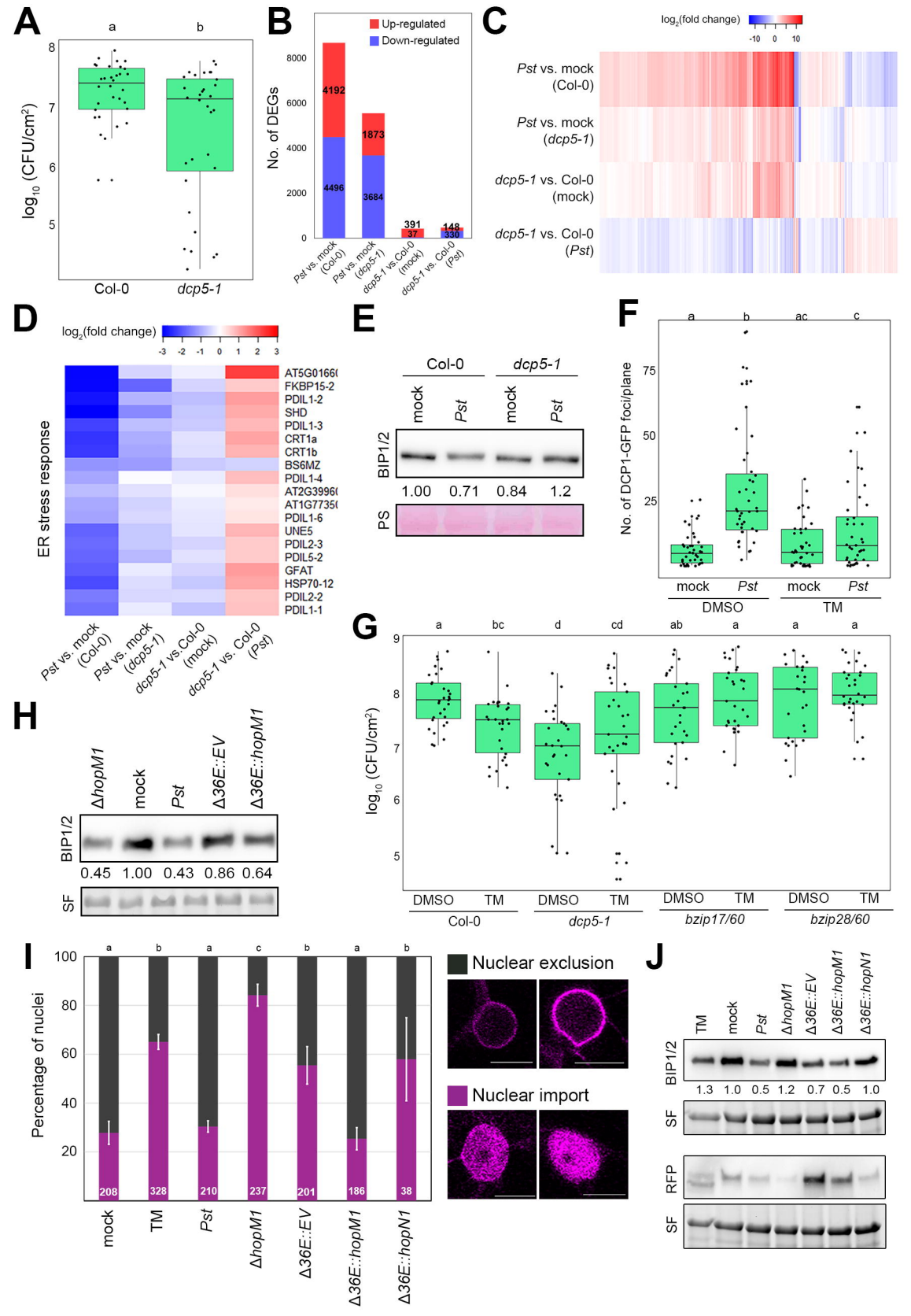
A
a
b
log10 (CFU/cm2)
Col-0
dcp5-1
B
Up-regulated
Down-regulated
No. of DEGs
4192
4496
1873
3684
391
37
148
330
Pst vs. mock (Col-0)
Pst vs. mock (dcp5-1)
dcp5-1 vs. Col-0 (mock)
dcp5-1 vs. Col-0 (Pst)
C
log2(fold change)
Pst vs. mock (Col-0)
Pst vs. mock (dcp5-1)
dcp5-1 vs. Col-0 (mock)
dcp5-1 vs. Col-0 (Pst)
D
log2(fold change)
ER stress response
AT5G0166(
FKBP15-2
PDIL1-2
SHD
PDIL1-3
CRT1a
CRT1b
BS6MZ
PDIL1-4
AT2G3996(
AT1G7735(
PDIL1-6
UNE5
PDIL2-3
PDIL5-2
GFAT
HSP70-12
PDIL2-2
PDIL1-1
E
Col-0
dcp5-1
mock
Pst
BIP1/2
1.00 0.71 0.84 1.2
PS
F
No. of DCP1-GFP foci/plane
mock
Pst
DMSO
TM
G
log10 (CFU/cm2)
DMSO
TM
Col-0
dcp5-1
bzip17/60
bzip28/60
H
ΔhopM1
mock
Pst
Δ36E::EV
Δ36E::hopM1
BIP1/2
0.45 1.00 0.43 0.86 0.64
SF
I
Percentage of nuclei
mock
TM
Pst
ΔhopM1
Δ36E::EV
Δ36E::hopM1
Δ36E::hopN1
Nuclear exclusion
Nuclear import
J
TM
mock
Pst
ΔhopM1
Δ36E::EV
Δ36E::hopM1
Δ36E::hopN1
BIP1/2
1.3 1.0 0.5 1.2 0.7 0.5 1.0
SF
RFP
SF

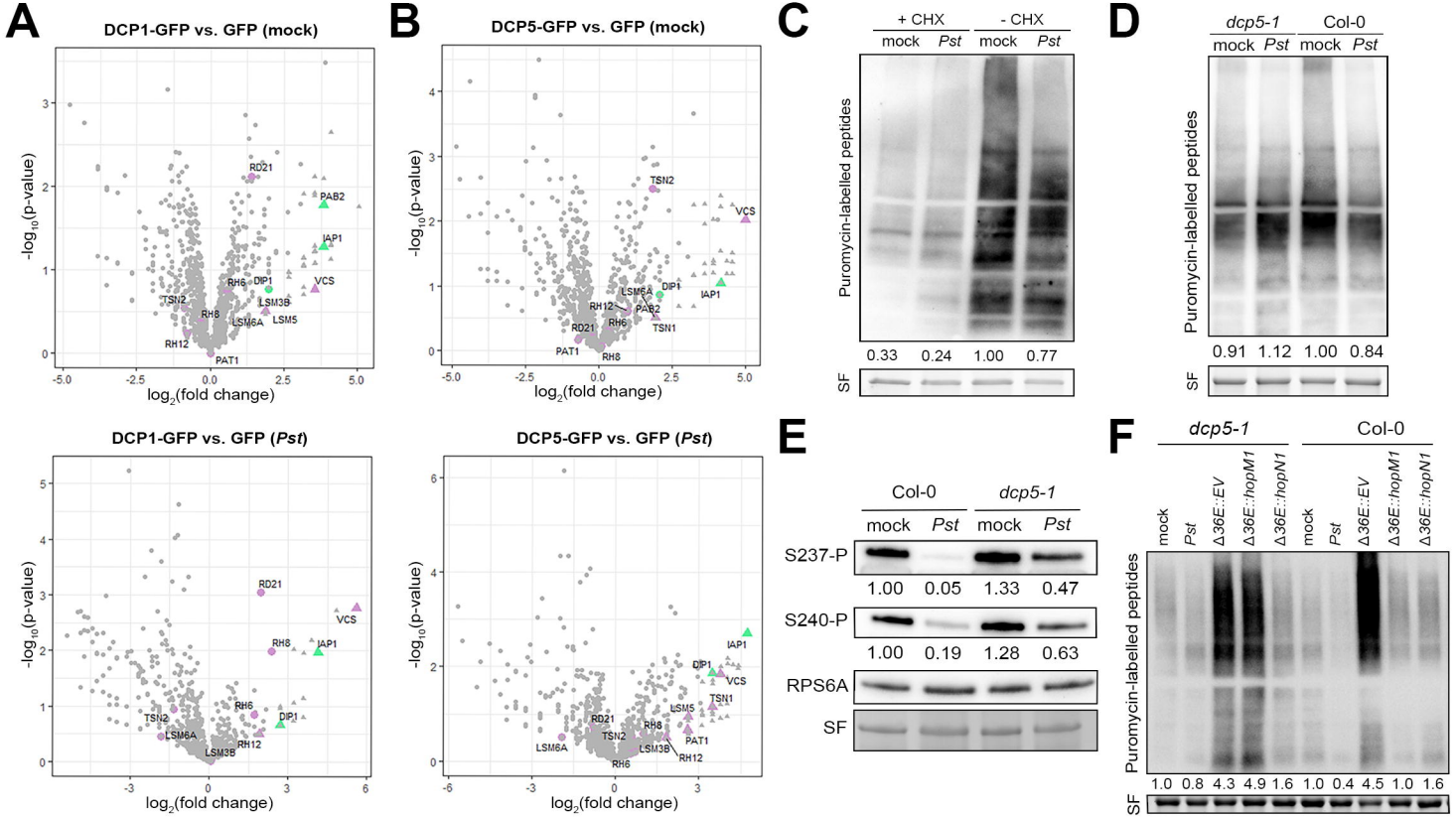
A
DCP1-GFP vs. GFP (mock)
-log10(p-value)
log2(fold change)
RD21
PAB2
IAP1
VCS
RH6
DIP1
TSN2
LSM3B
RH8
LSM6A
LSM5
RH12
PAT1
DCP1-GFP vs. GFP (Pst)
B
DCP5-GFP vs. GFP (mock)
TSN2
VCS
LSM6A
DIP1
IAP1
RH12
PAB2
RH6
TSN1
RD21
PAT1
RH8
DCP5-GFP vs. GFP (Pst)
C
+ CHX
- CHX
mock
Pst
mock
Pst
Puromycin-labelled peptides
0.33 0.24 1.00 0.77
SF
D
dcp5-1
Col-0
mock
Pst
mock
Pst
Puromycin-labelled peptides
0.91 1.12 1.00 0.84
SF
E
Col-0
dcp5-1
mock
Pst
mock
Pst
S237-P
1.00 0.05 1.33 0.47
S240-P
1.00 0.19 1.28 0.63
RPS6A
SF
F
dcp5-1
Col-0
mock
Pst
Δ36E::EV
Δ36E::hopM1
Δ36E::hopN1
mock
Pst
Δ36E::EV
Δ36E::hopM1
Δ36E::hopN1
Puromycin-labelled peptides
1.0 0.8 4.3 4.9 1.6 1.0 0.4 4.5 1.0 1.6
SF

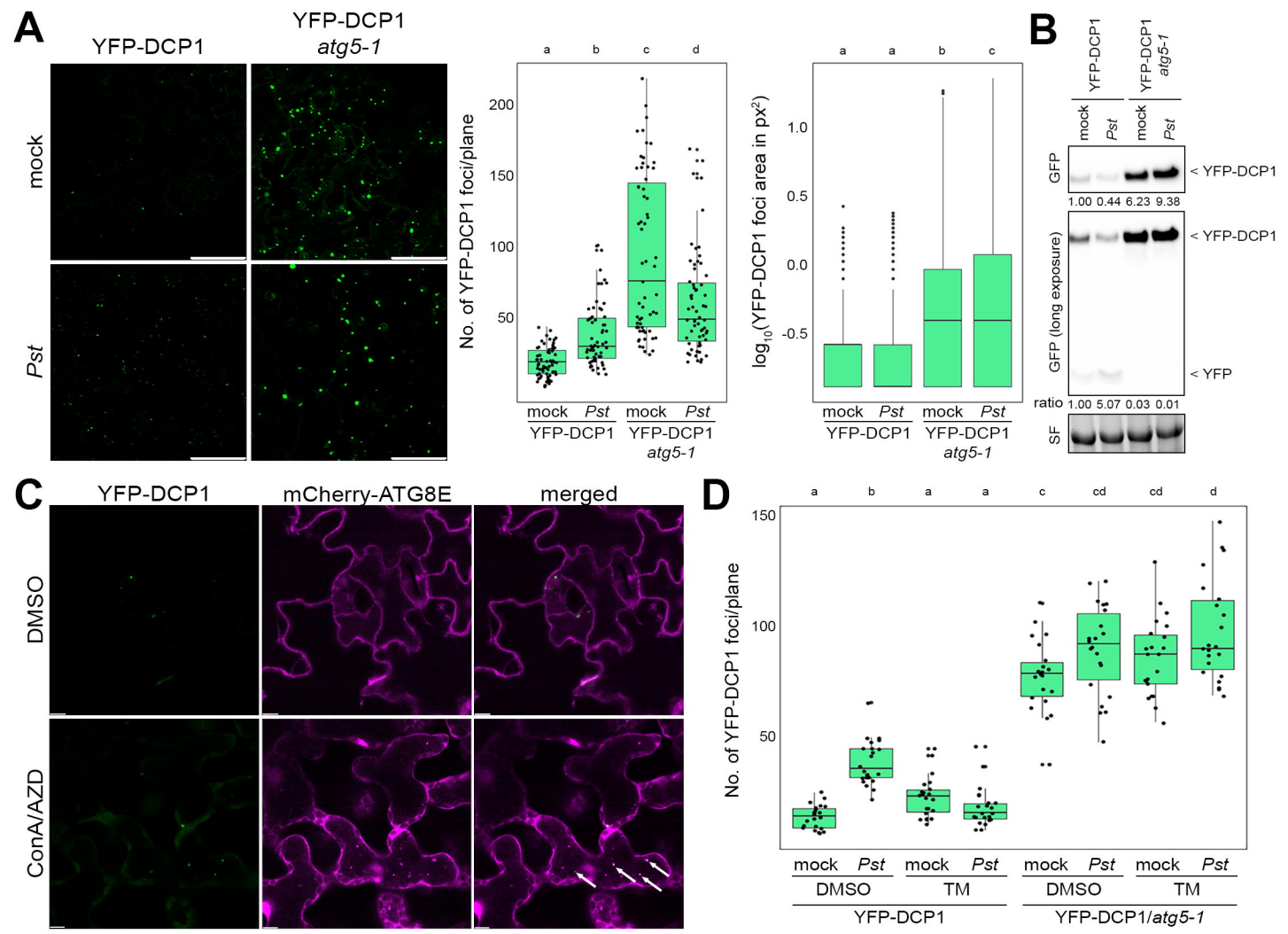
A
YFP-DCP1
YFP-DCP1
atg5-1
mock
Pst
No. of YFP-DCP1 foci/plane
log10(YFP-DCP1 foci area in px2)
mock Pst mock Pst
YFP-DCP1 YFP-DCP1
atg5-1
B
YFP-DCP1
YFP-DCP1
atg5-1
GFP
GFP (long exposure)
< YFP-DCP1
< YFP
1.00 0.44 6.23 9.38
ratio 1.00 5.07 0.03 0.01
SF
C
YFP-DCP1
mCherry-ATG8E
merged
DMSO
ConA/AZD
D
No. of YFP-DCP1 foci/plane
mock Pst mock Pst mock Pst mock Pst
DMSO TM DMSO TM
YFP-DCP1
YFP-DCP1/atg5-1

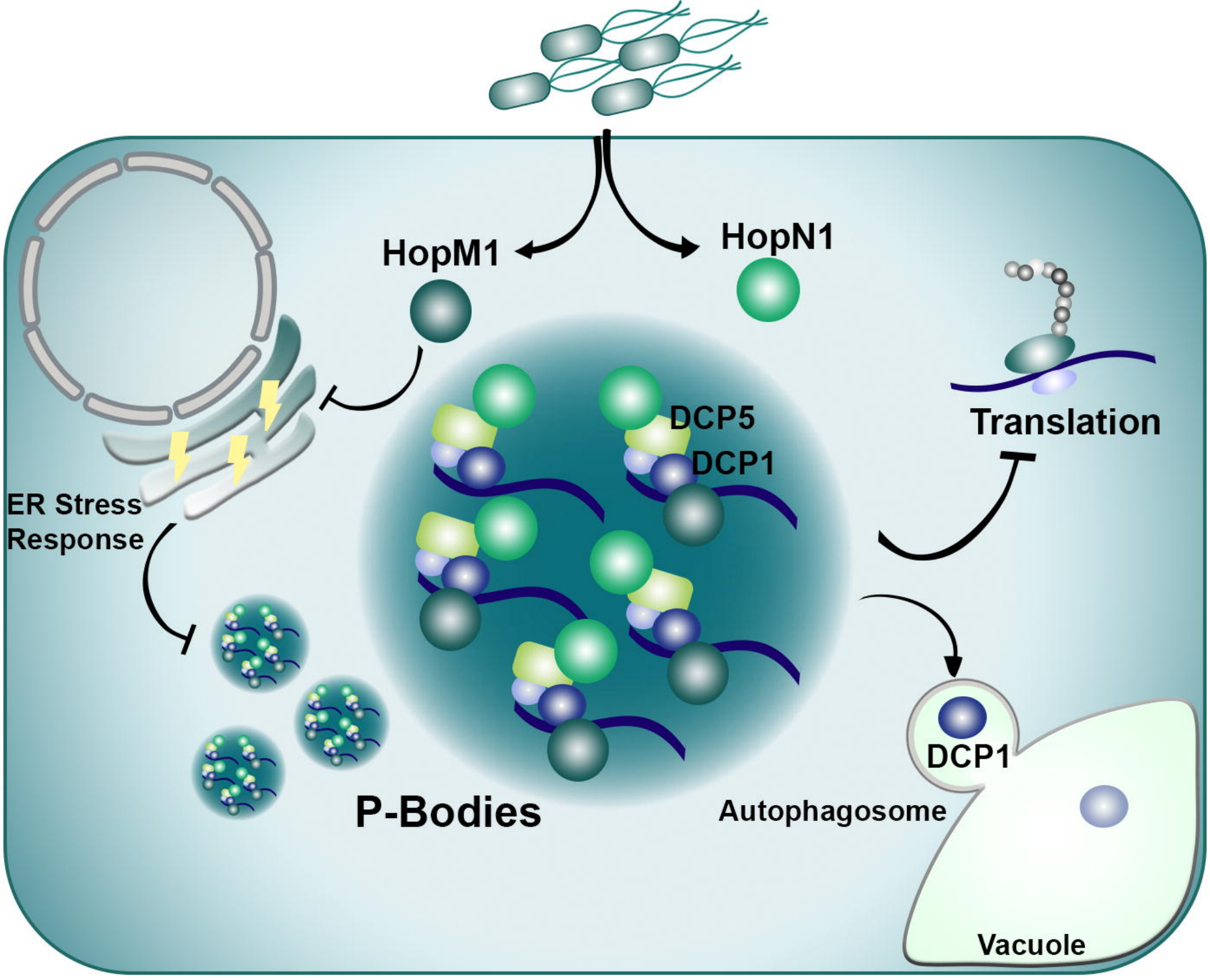
HopM1
HopN1
DCP5
DCP1
Translation
ER Stress
Response
P-Bodies
Autophagosome
DCP1
Vacuole